THE EFFECT OF UNIFORM AND NON-UNIFORM ELECTRON DENSITY MODELS FOR DETERMINING SHOCK SPEED OF A TYPE II SOLAR RADIO BURST

D .P .S .Nilagarathne

Index Number: 2985

A thesis submitted to the Department of Physical Sciences, Rajarata University of Sri Lanka in partial fulfillment of the requirements for the award of the B.Sc. (Four Year) degree in Applied Sciences

Department of Physical Sciences

Faculty of Applied Sciences

Rajarata University of Sri Lanka

Mihintale – Sri Lanka

January, 2019

CERTIFICATION OF THE SUPERVISORS

This is to certify that the thesis on "THE EFFECT OF UNIFORM AND NON-UNIFORM ELECTRON DENSITY MODELS FOR DETERMINNING SHOCK SPEED OF A TYPE II SOLAR RADIO BURST" is completed by **D.P.S.Nilagarathne** in partial fulfillment of the requirements for the award of the B. Sc. (Four Year) degree in Applied Sciences. The *bona fide* work reported in this thesis has been carried out successfully under our supervision.

……

Dr. Harshani Wijewardane

Senior Lecturer

Department of Physical Sciences

Faculty of Applied Sciences

Rajarata University of Sri Lanka

Mihintale

Date:

……

Janaka Adassuriya

Research Scientist

Astronomy & Space Science Division

Arthur C Clarke Institute

Katubedda,

Moratuwa

Sri Lanka

Date:

……

Dr. U. Dahanayake

Head

Department of Physical Sciences

Rajarata University of Sri Lanka

Mihintale

Date:

DECLARATION

I hereby do solemnly declare that the work presented in this thesis has been carried out by me and has not been previously submitted to any other University/ College/ Organization for an academic qualification/ certificate/ diploma or degree.

The work I have presented does not breach any copyright.

……

D. P. S. Nilagarathne

No: 728/A, Bloemendhal Road,

Colombo 15.

Date:

ACKNOWLEDGEMENTS

First and foremost I would like to convey my deepest gratitude to Dr. H.O.Wijewardane, senior lecturer, Department of Physical Sciences, Faculty of Applied Sciences, Rajarata University of Sri Lanka for encouraging me by providing her glorious knowledge and for her continuous guidance which assisted me in completing my whole career successfully so far.

I would like to extend my sincere thanks to Mr. Janaka Adassuriya, Research Scientist, Astronomy & Space Science Division, Arthur C Clarke Institute, for the dedication of his invaluable time on this work and for his generous support. Without his help, I wouldn't be able to finish this work.

Also, I would like to thank Arthur C Clarke Institute for Modern Technologies (ACCIMT), Katubedda, Moratuwa for giving this great opportunity for me to conduct my research.

I am thankful to the lecturers of the Department of Physical Sciences, Faculty of Applied Sciences, Rajarata University of Sri Lanka for giving their support to reach my goal.

My affectionate gratitude goes to my loving parents, sister, specially my brother D.N.Nilagarathne and Mr.K.S.C.Y.Bandara who gave me unconditional support to complete the research successfully.

Finally, I would like to impose my thanks to my friends and all the other people who helped me to complete this research successfully.

ABSTRACT

Solar flare is one of the solar activities bonded with the coronal mass ejections of the sun. It is a giant burst of x-rays, γ-rays, radio emissions and energy which travel at the speed of light in all directions. Emissions of radio waves create an important part for the solar radio burst. There are five types of radio bursts identified by the radio astronomers. Among the five types, type II radio burst, which is also called slow drift burst or shock waves have special features which are different from other radio burst types. The exact mechanism of type II burst is still a matter of debate. Therefore the determination of properties of solar radio bursts enhances our knowledge of understanding this natural phenomenon. Shock speed or plasma velocity is one of the valuable parameter that gives much information about solar radio bursts.

In this study, shock speed of type II radio burst was estimated. The estimation was done by the use of uniform density model and the non-uniform density model for the sun. The spectroscopic data needed for the study was obtained by the e-CALLISTO data base. e-CALLISTO is a global network of radio spectrometers operating in 24 hours to detect solar radio bursts originating from the sun. The result shows that there is a significant change in shock speed with the non-uniform electron density model. The rate of increase in shock speed with the altitude in non-uniform model is less than that of the uniform model. The shock speed is proportional to the electron density (N_e) and inversely proportional to the rate of change in electron density with altitude (dN_e/dr). The determined shock speed for the altitude of one solar radius is 2131 km/s for uniform model and 766 km/s for non-uniform model. The shock speed for uniform electron density model is quite higher than the non-uniform model. Hence, the shock speed calculated by the non-uniform density model which accounts for the actual electron destitution needed to be use in further investigations of Type II solar bursts.

TABLE OF CONTENTS

ACKNOWLEDGEMENTS iii
ABSTRACT iv
TABLE OF CONTENTS v
LIST OF ABBRIVIATIONS vii
LIST OF FIGURES viii
LIST OF TABLES x
CHAPTER 01 1
INTRODUCTION AND OVERVIEW 1
1.1 Solar flares 2
1.2 Solar radio burst types 4
1.3 Type II solar radio burst 6
1.4 e-CALLISTO spectrometer 8
CHAPTER 02 10
THEORY 10
2.1 Uniform electron density model 11
2.2 Non-uniform electron density model 11
CHAPTER 03 14
MATERIALS AND METHODS 14
3.1 Uniform electron density model 15
3.1.1 Analysis of electron density (N_Q) 15
3.1.2 Analysis of frequency (f) 18
3.2 Non-uniform electron density model 22
3.2.1 Analysis of electron density (N) 22
CHAPTER 04 38
RESULTS AND DISCUSSION 38

4.1 Shock speed for uniform density model 38
4.2 Shock speed for non-uniform density model 40
4.3 Comparison between uniform and non-uniform density models 41
REFERENCES 43

LIST OF ABBRIVIATIONS

CME – Coronal Mass Ejections

FITS – Flexible Image Transport System

IRAF – Image Reduction and Analysis Facility

LIST OF FIGURES

Figure 1. 1: Solar flare 3

Figure 1. 2: Variation of patterns of solar bursts 5

Figure 1. 3: Type II solar radio burst with harmonic observed at OOTY observatory; India .. 7

Figure 1. 4: Type II solar radio burst with harmonics and “herring-bones” observed at ROSWELL-NM observatory; USA 7

Figure 1. 5: Basic schematic diagram of CALLISTO spectrometer..... 9

Figure 2. 1: ‘P’ represents the point where the flare occurred in 3D view of sun……...12

Figure 3. 1: Type II solar radio burst observed at ROSWELL-NM observatory; USA……..14

Figure 3. 2: N_Q vs r graph for active sun 15

Figure 3. 3: dN/dr vs r graph for active sun 16

Figure 3. 4: N_Q vs r graph for quiet sun 16

Figure 3. 5: dN/dr vs r graph for quiet sun 17

Figure 3. 6: Contour plot of full flare 18

Figure 3. 7: Contour plot of cropped flare 19

Figure 3. 8: Frequency channel vs time graph with all points 20

Figure 3. 9: Frequency channel vs time graph with removed points 20

Figure 3. 10: Frequency vs time graph after converted to actual frequency value 21

Figure 3. 11: Maximum pixel values vs x coordinate graph..... 24

Figure 3. 12: Maximum pixel values vs x coordinate graph..... 26

Figure 3. 13: 5×5 error matrix..... 26

Figure 3. 14: Sum of pixel values vs time graph 28

Figure 3. 15: 2D image of sun 29

Figure 3. 16: The area covered by red colour circle shows the changed area 29

Figure 3. 17: Previous origin by considering (0,0) to be in the corner of the image 30

Figure 3. 18: Expected origin considering (0,0) to be in the middle of the image 31

Figure 3. 19: Origin of the image loaded to matlab software 32

Figure 3. 20: The point which the solar flare was occurred has been shifted to the fourth quadrant..... 33

Figure 3. 21: 270° degrees rotated image 34

Figure 3. 22: The point that is in red is where we have considered the origin and the point that is in green is the point that the flare has occurred..... 35

Figure 3. 23: N vs r graph 36

Figure 3. 24: dN/dr vs r graph..... 37

Figure 4. 1: V vs r curve for uniform electron density model of quiet sun…….. 38

Figure 4. 2: V vs r curve for uniform electron density model of active sun 39

Figure 4. 3: V vs r curve for non-uniform electron density model 40

Figure 4. 4: Velocity curves of uniform and non-uniform electron density models..... 41

LIST OF TABLES

Table 3. 1: Maximum pixel values of the successive images 23

Table 3. 2: Pixel values at the reference point (454,452) 25

Table 3. 3: Sum of pixel values in the matrix 27

CHAPTER 01

INTRODUCTION AND OVERVIEW

The solar flares are one of the activities of solar system that occurs with the change of solar magnetic field. Generally, it is a non-thermal emission and the change is started with the collision of energetic charged particles with magnetic field, electric field and plasma radiation. These energetic charged particles are protons, electrons and heavy ions. Solar radio bursts are structure of the frequencies that changes with time due to release of magnetic energy associated with sunspots. According to the radio astronomy the frequencies of solar radio bursts vary from 70 MHz to 2.2 GHz. Yet most of the solar radio bursts occur in a low frequency range such as 200MHz [1, 2]. Normally, this low frequency emission is considered to be a radio emission. Radio burst types will be discussed on Chapter 1.2.

The exact mechanism of type II burst is still a matter of debate; hence it was selected for the study. Shock speed or plasma velocity is one of the valuable parameter that gives much information about solar radio bursts. Normally the calculation of the shock speed was done by uniform electron density model, where one considers the electron density around the sun to be constant. In a non-uniform electron density model the electron density is considered to be varied in the active regions. Although there are many work of shock speed of the type II solar burst calculated from uniform electron density model, the shock speed calculation from non-uniform electron density model is an ongoing research. Therefore the work describe here represents the results of the shock speed of type II radio burst compared with both uniform and non-uniform model. The continuation of this chapter in the thesis will give a general introduction about solar flares, types of radio bursts and the e-CALLISTO spectrometer. Chapter 02 will give the theoretical background needed for calculation, chapter 03 consists of the methodologies that have been used, chapter 04 give the observations and chapter 05 give the conclusion and discussion.

1.1 Solar flares

Solar flares are the most active incidence of solar activities and, it contributes for the solar radio astronomy. It is a huge explosion in solar atmosphere that occur suddenly and release incalculable energy in a short time period. The released energies are super thermal energies. The released energy with acceleration of electrons can be observed indirectly as x-ray, γ-ray and radio emissions. Similar to other solar activities solar flare also change the solar magnetic field. In radio astronomy, solar radio burst is the first identified phenomenon around the sun. Solar flares act an important role of the space weather conditions [3,4]. There is a close connection between solar flares and Coronal Mass ejections (CME). CME is also an event that happens around the sun. Both flares and CME's accelerate ions and electrons. CME is a huge burst that can be observed in coronal structure in time to time that do changes to the Earth's magnetosphere. There is an interconnection with solar flares and coronal mass ejections. It has direct relationship with type II solar burst. CME emits the large scale density waves such as radio waves. Due to that it may change the Earth's magnetic field. Solar events and Earth's environment have close relationship. By solar radio burst we can identify the solar activities such as level of the radiation that emits by the sun, etc. Solar flares are classified based on the size and the brightness in specific wavelengths. Considering the X-ray emission, flares are classified into five categories namely A, B, C, M and X from weak to strong [3,5].

Nowadays flares are divided into two types called "low temperature flares" and "high temperature flares" which differ from their physical properties and with the methods of observation used to record them. The life time of solar flares is very short-lived. The small flares have seconds to a few minutes while the large ones may have maximum of few hours.

There are several type of flares, namely plage flare or confined flare, white light flare, limb flare, flare kernels or hot cores, two-ribbon flare or two-strand flare, hyder flare or impact flare, homologous flare, flare-associated phenomena, moreton wave [6]. A large flare releases about 10^{25} J energy. This energy is equivalent to bomb of 2 billion megatons and temperature with 2×10^{7} K [7]. A picture of a solar flare is given in the Figure 1.1.

Figure 1.1: Solar flare

1.2 Solar radio burst types

Solar radio bursts are identified by the e-CALLISTO spectrometer which is operating in 24 hours to detect solar radio bursts originating from solar flares. This global network e-CALLISTO has the spectroscopic data in its database to investigate the parameters of solar radio burst [8]. By analyzing the data observed from the CALLISTO spectrometer, researchers have classified five types of radio bursts. These classifications have done based on the frequency ranges and temporal variations. The types are, Type I - Noise storm, Type II - Slow drift burst or shock waves, Type III - Fast drift burst or electron beams, Type IV - Broadband quasi continuum emission or trapped electrons, Type V –Continuum emissions at meter wavelength [9,10]. Among these five types, Type I can be identified in the frequency range of 80-200 MHz, Type II in the range of 20-150 MHz, Type III in the range of 10 kHz-1GHz, Type IV in 20 MHz - 2GHz and Type V in the frequency range 10-200 MHz. In these five types, there is a variety with the pattern of the flares. The figure 1.2 shows the variation of pattern in all five types and how it was detected to CALLISTO spectrometer. Figure 1.2(a) gives the type I noise storm observed at DARO-HF observatory; Germany. Figure 1.2(b) gives type II slow drift burst observed at ALMATY observatory; Kazakhstan. Figure 1.2(c) gives type III fast drift burst observed at BLEN5M observatory; Switzerland. Figure 1.2(d) gives type IV burst observed at BLEN7M observatory; Switzerland and Figure 1.2(e) gives type V burst observed at BLEN7M observatory; Switzerland.

Type I burst

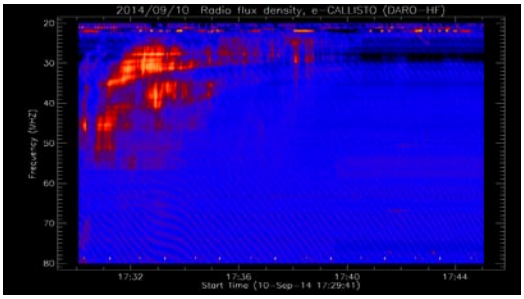

Figure (a): Type I noise storm observed at DARO-HF observatory; Germany

Type II burst

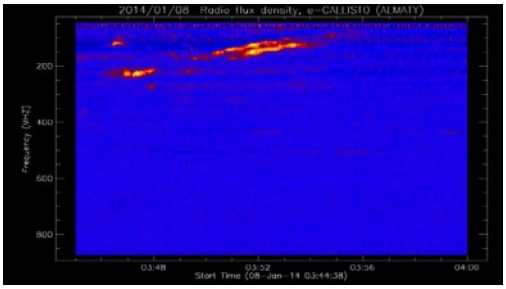

Figure (b): Type II slow drift burst observed at ALMATY observatory; Kazakhstan

Type III burst

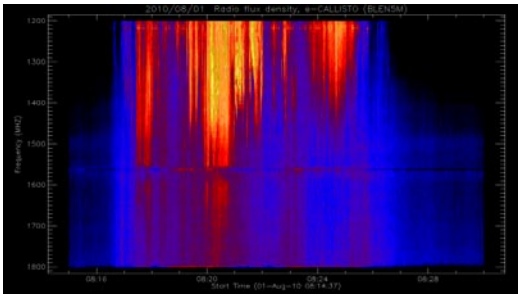

Figure (c): Type III fast drift burst observed at BLEN5M observatory; Switzerland

Type IV burst

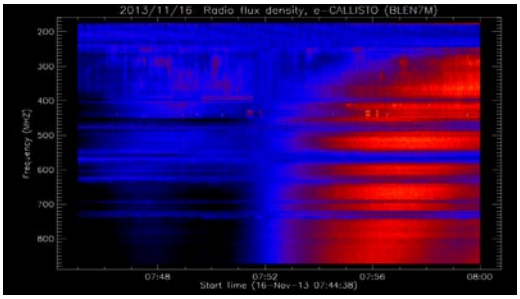

Figure (d): Type IV burst observed at BLEN7M observatory; Switzerland

Type V burst

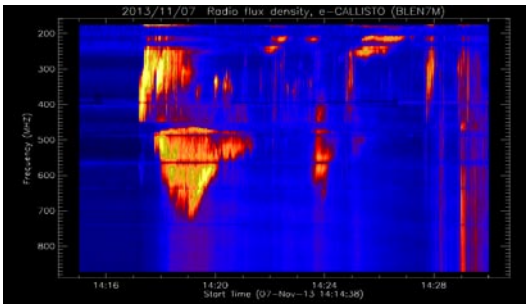

Figure (e): Type V burst observed atBLEN7M observatory; Switzerland

Figure 1.2: Variation of patterns of solar bursts

These all five types of solar burst again categorized into five categories namely A,B,C,M and X depending on the x-ray flux. Here “A” has the weakest x-ray flux and “X” has the strongest x-ray flux [3].

1.3 Type II solar radio burst

Type II solar radio burst are slowly drifting bands often in pairs from high to low frequency in the dynamic spectra. It has special features and special characters that change from the other types of solar radio bursts. Normally, type II burst are low frequency events that can be detected below 100 MHz. It may have random polarization or complex polarization structures. There is a tight correlation between type II radio burst and CME. The energy distribution of type II burst is vary within 1.506×10^{-6} to 6.906×10^{-6} eV [5,11]. Primitively, type II burst start after beginning of a flare within 2-15 minutes and end about 10-15 minutes in the meter region. Slow drift bursts such as type II bursts are automatically associated with large flare events. In type II bursts, there are special structures that can be identified. They are Harmonic radiation, Frequency splitting and Herring-Bone structure. Harmonic structure has built with the existence of harmonic radiation in connection with narrow-band structures which can be identified more than half of type II bursts in the meter region. This can be recognized in dynamic spectra. In the frequency splitting structure, type II bursts varies by the effect of frequency or band splitting and herring-bone structure is the most common structure among these three types. Figure 1.3 shows the harmonic radiation and Figure 1.4 shows the herring-bone structure.

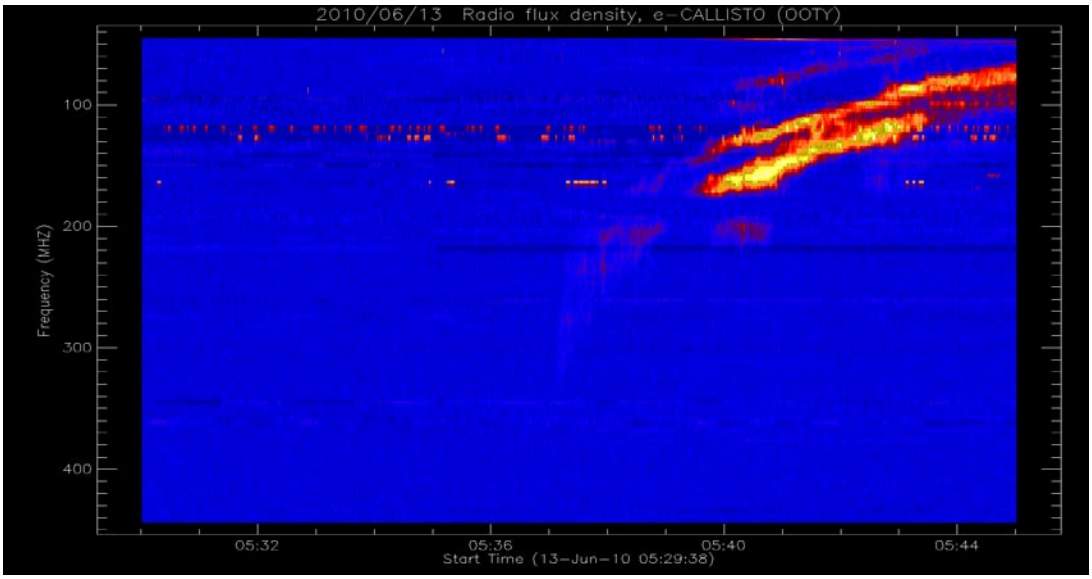

Figure 1.3: Type II solar radio burst with harmonic observed at OOTY observatory; India

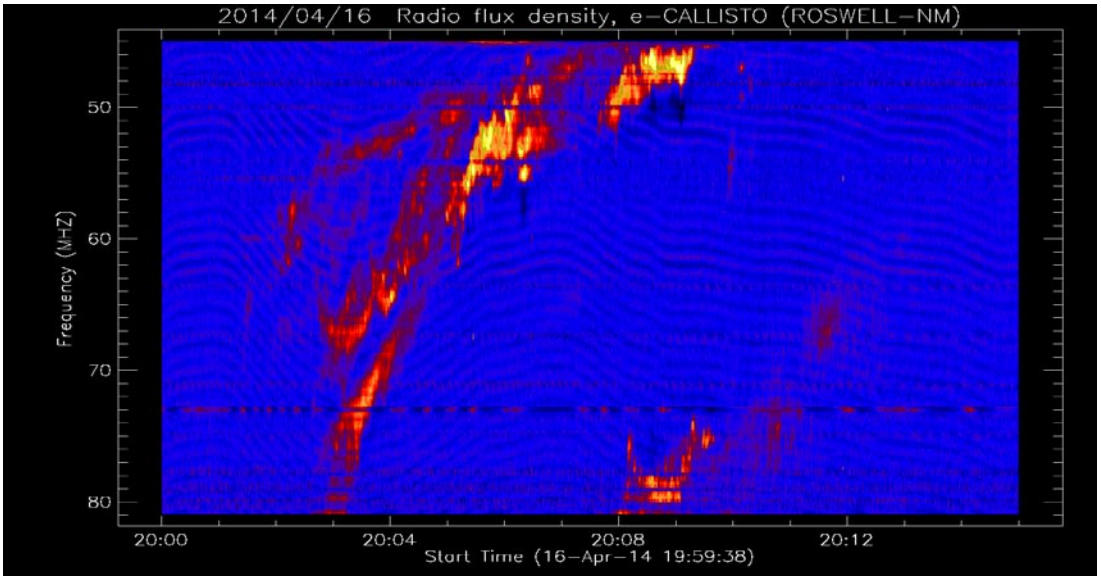

Figure 1.4: Type II solar radio burst with harmonics and “herring-bones” observed at ROSWELL-NM observatory; USA

1.4 e-CALLISTO spectrometer

The observations that are gained from the satellites of solar particles, x-rays, extreme UV and by white-light coronal emission are used for the investigation of the sun. Dynamics of solar corona is also a matter to be discussed since it creates many new phenomenon with the time. The plasma phenomena emitting radio waves, may be the basic factor that gives the specific idea of solar activities like solar radio bursts which can be observed by the ground based telescopes such as e-CALLISTO spectrometer [8].

E-CALLISTO is a radio spectrometer which is operating in 24 hours to detect solar radio bursts originating from solar flares. There are more than 150 instruments at more than 90 locations worldwide. All CALLISTO spectrometers combined and create the e-CALLISTO network. CALLISTO stands for compound astronomical low cost low frequency instrument for spectroscopy and transportable observatory. It is a programmable heterodyne receiver built in the framework of IHY2007 and ISWI (International Space Weather Initiative) by former Radio and Plasma Physics Group at ETH Zurich, Switzerland. Generally, this is applicable for observation of solar radio bursts and rfi-monitoring for astronomical science, education and outreach. The main advantage of this spectrometer is the cost. It costs very little for hardware and software. Total frequency range of the instrument is from 45-870 MHz and an individual channel has 300 kHz bandwidth. It has frequency resolution of 62.5 kHz which can be controlled by software. The data exact as FIT-file with up to 400 frequencies per sweep. Copies can be simply made and can be broadcast to other locations. All FITS files consists of data during 15 minutes observations of the whole spectrum. Time resolution is 800 pixels per second. IDL-, PERL- and python-routines were written for proper data handling [12]. Figure 1.5 gives a basic schematic diagram of CALLISTO spectrometer.

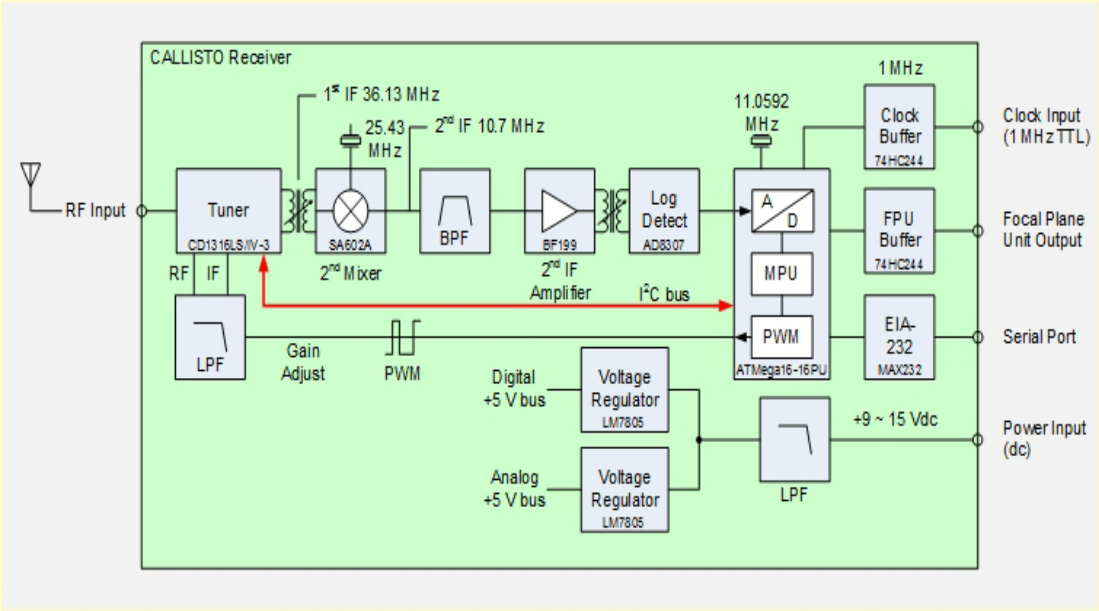

Figure 1.5: Basic schematic diagram of CALLISTO spectrometer

CHAPTER 02

THEORY

The theory which was used for the calculation in the work on this thesis was three fold. First, how to calculate the shock speed, then the shock speed was calculated using two different models, uniform and non-uniform electron density. The theory that was used for the calculation is described in this chapter. The shock speed for uniform and non-uniform electron density models can be calculate by using the equation 2.1 as shown below.

$$V = \frac{2N\frac{df}{dt}}{f\frac{dN}{dr}} \qquad 2.1$$

Where,

V - shock speed

N - electron density

f - plasma frequency

$\frac{df}{dt}$ - drift rate

$\frac{dN}{dr}$ - change of electron density with respect to height

In the above equation, different models can be used to calculate the electron density N.

2.1 Uniform electron density model

There are several coronal density models which describe the electron density over chromosphere with uniform electron density model approach. Newkirk model is one of the best model [13,14]. Newkirk model has included the electron density with respect to the distance from the center of the sun in the quiet and active conditions. He assumed that the variation of electron density in the quiet and active sun is uniform in the specific distance from the center of the sun. Electron density of the quiet sun is Newkirk×1 and active sun is Newkirk×20 [13]. The Newkirk equation is given by 2.2.

$$N_Q = N_0 \times 10^{4.32/R} \quad (2.2)$$

Where,

N_Q – electron density for quiet sun.

N_0 - 4.2×10^4

R – distance from the center of the sun in units of the solar radius.

2.2 Non-uniform electron density model

In the non-uniform electron density model, a departure from the spherical symmetry is determined by the presence of an active region. The gradient of the electron density above the active region is steeper than the gradient of the quiet corona. As a result, the electron density around the sun is not uniform. So a new model was introduced to calculate the electron density above the active region of the sun when it is not uniform [14]. The model for the electron density at any spot in the corona is shown below.

$$N(R, \beta) = N_Q(\mathrm{R})\,[1+C_1 e^{-(\frac{\beta^2}{2\sigma^2})}] \quad (2.3)$$

Where,

$N(R, \beta)$ - electron density at distance R from the solar center

N_Q - Newkirk model

β - chord between a point on the axis of the active region and distance R from the center of the sun

C_1 - a constant

σ - a dispersion parameter

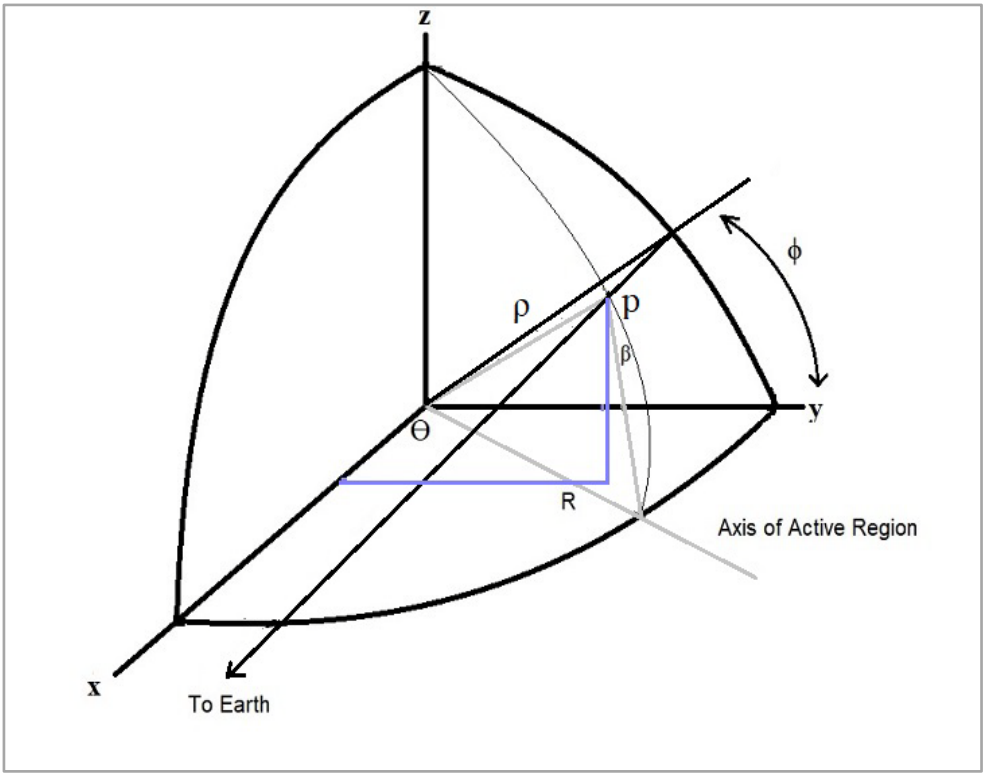

Figure 2.1: 'P' represents the point where the flare occurred in 3D view of sun

Here, $\beta^2 = (x - R\cos\theta)^2 + (y - R\sin\theta)^2 + z^2$ 2.4

X axis is directed towards the earth and the xy-plane contains the axis of the active region. According to the Figure 2.1, P is the point where the flare has occurred. The point P had been shown by x, y, z coordinates in 3D space. β was also introduced regarding the coordinates of the point P and the radius of the sun.

By the calculations done by Newkirk, the values for the parameters are adopted as C_1 = 0.97 and σ = 0.235. When consider the limb of the active region θ becomes 90° and therefore equation 2.4 can be reduced to,

$$\beta^2 = x^2 + (y - R)^2 + z^2 \qquad 2.5$$

The above mentioned two models for density have been used for the calculation of shock speed and a comparison was done for the both models.

CHAPTER 03

MATERIALS AND METHODS

The type II radio bursts data that have been taken from CALLISTO spectrometer were used to carry-on this research. Data were taken from lmsal.com which was published by the website in 16th of April 2014. Fits file which refers to the event happened was taken from e-CALLISTO website. The observation taken by "ROSWELL-NM observatory; USA" of type II solar burst which was captured at 19:59:38 were used here. Among five types of solar flare classes M class type was taken to further analysis. Then, plasma velocity of uniform electron density model and non-uniform electron density model was calculated. Matlab software was used to analyze the data.

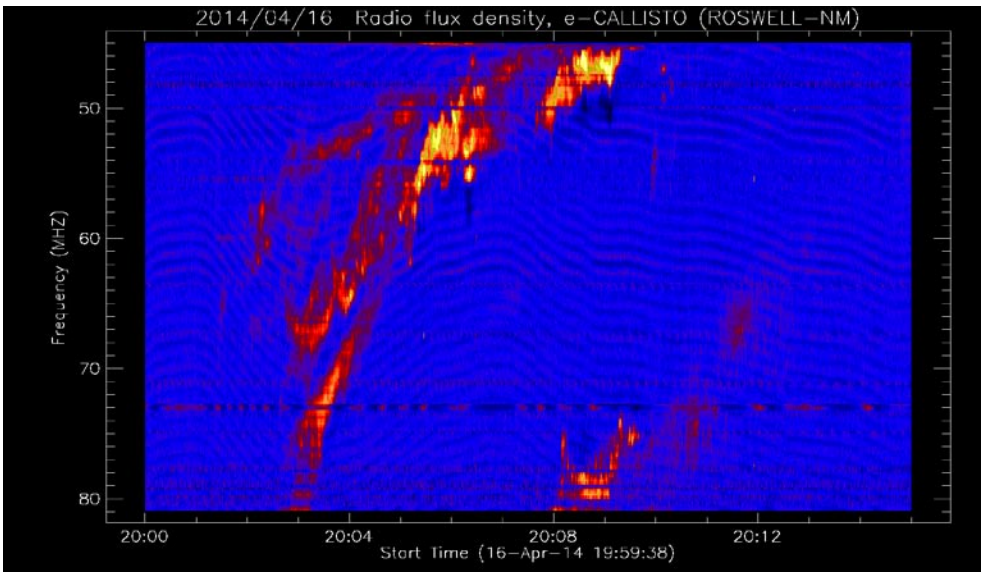

Figure 3.1: Type II solar radio burst observed at ROSWELL-NM observatory; USA

3.1 Uniform electron density model

3.1.1 Analysis of electron density (N_Q)

To calculate the electron density, Newkirk model was used. Distance from the sun varied between 1.0 to 3.0 in 0.1 steps and electron density for different r values were obtained for the quiet sun and it was multiplied by 20 to obtain the electron density of the active sun. The calculation was done using Excel software. N_Q vs r graphs were plotted separately for quiet and active sun to observe the variation. Then $\frac{dN}{dr}$ values for different 'r' values were obtained from matlab software. Here, $\frac{dN}{dr}$ values were calculated considering the electron density as a power function, because in the equation which has been derived by Newkirk, the electron density has been considered as a power function. $\frac{dN}{dr}$ vs r was plotted for the two states of the sun. N_Q vs r and $\frac{dN}{dr}$ vs r graphs for active and quiet sun are given in the Figures 3.2, 3.3, 3.4 and 3.5 respectively.

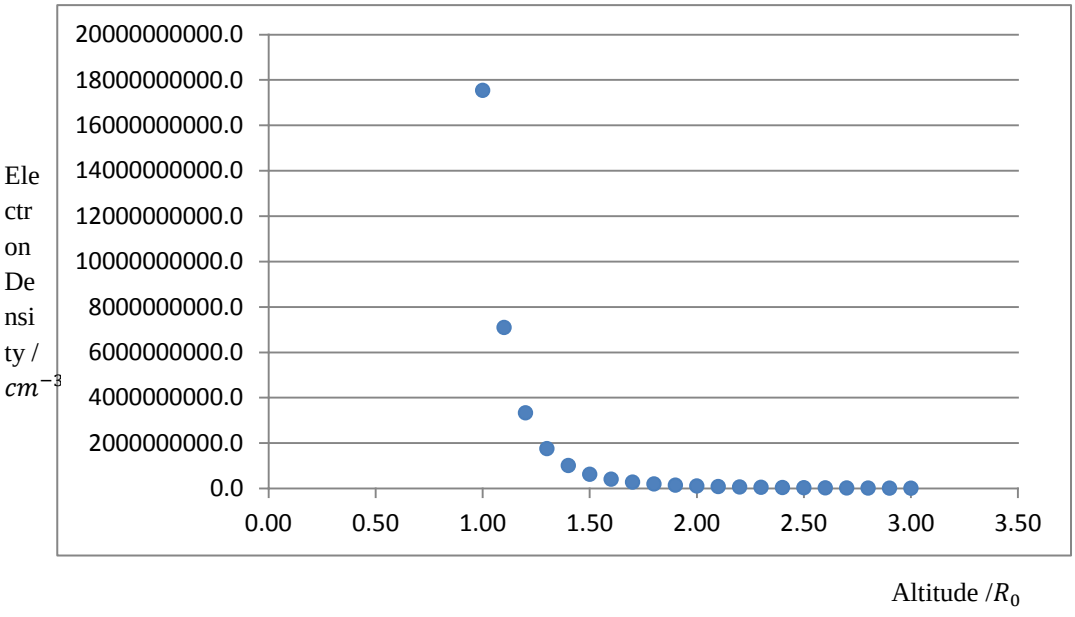

Figure 3.2: N_Q vs r graph for active sun

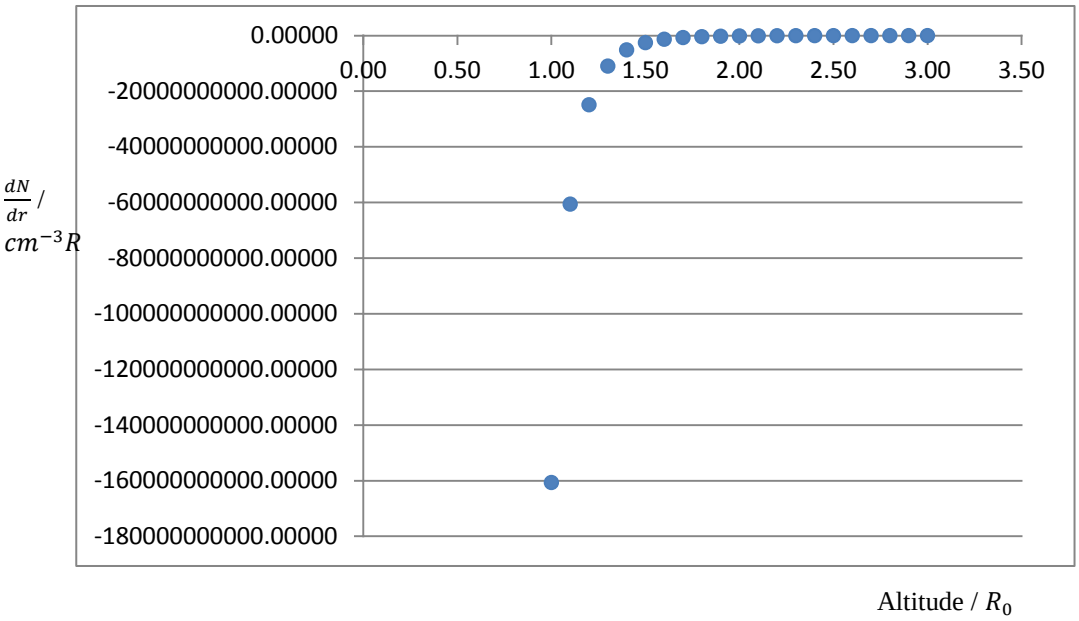

Figure 3.3: $\frac{dN}{dr}$ vs r graph for active sun

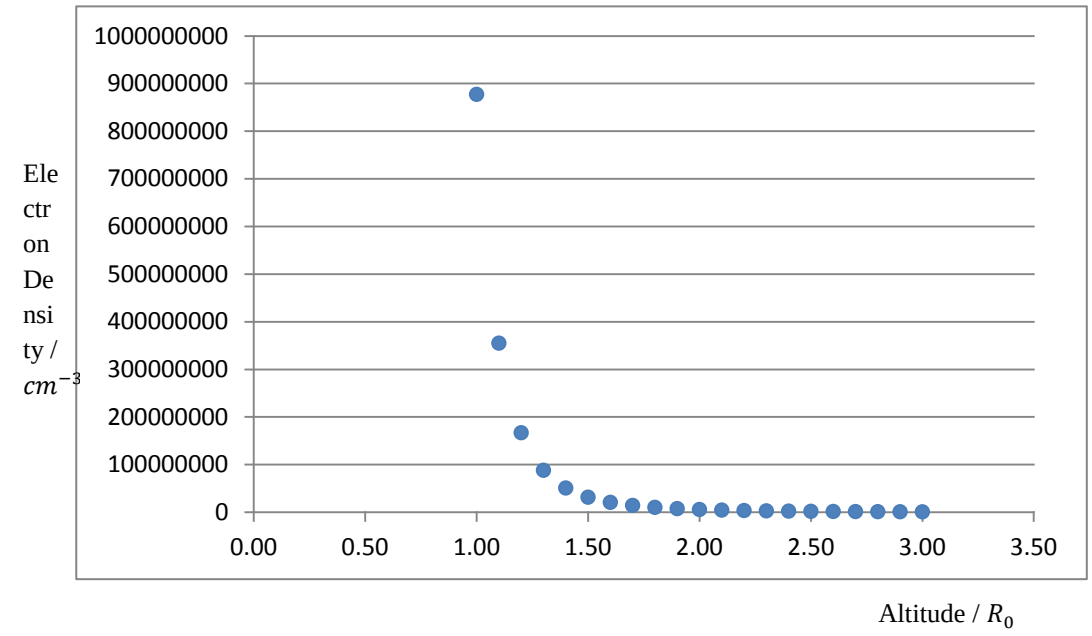

Figure 3.4: N_Q vs r graph for quiet sun

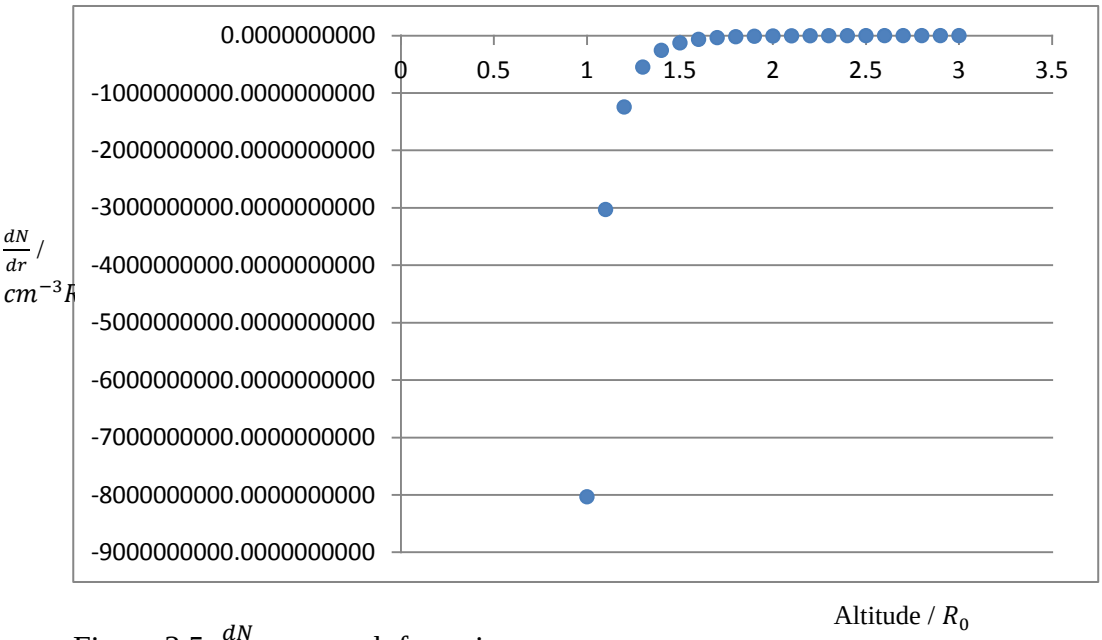

Figure 3.5: $\frac{dN}{dr}$ vs r graph for quiet sun

3.1.2 Analysis of frequency (*f*)

At the beginning of the analysis, FITS file of the flare image was read using matlab command. Unwanted noises were identified in the image. So, to remove the unnecessary noises of the flare image, fits file of a blank image which was captured few hours later the flare image was captured was read using matlab command. Then, the blank image was subtracted from the flare image to remove the other noise frequencies of the flare image and noise extracted flare was gained. Then the subtracted image was cropped using matlab software and the solar radio burst part was isolated. Contour plots of the full flare and cropped flare were shown in Figure 3.6 and Figure 3.7 respectively.

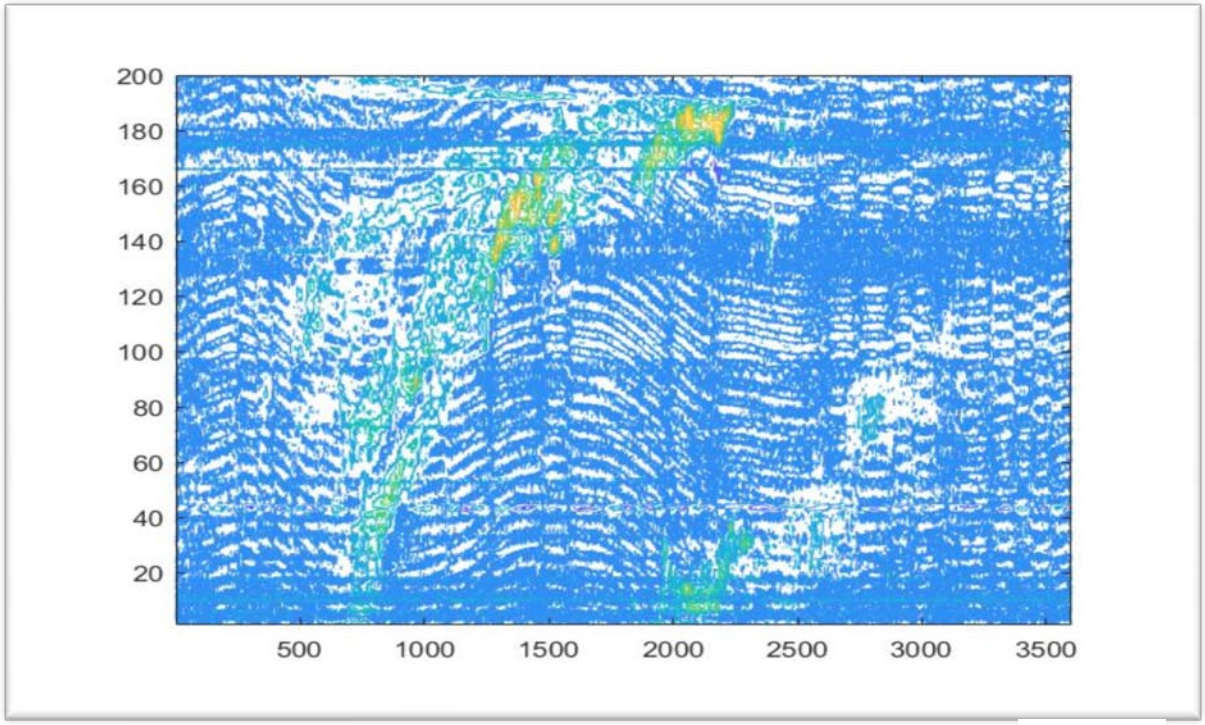

Figure 3.6: Contour plot of full flare

Normally, in the images taken from the CALLISTO spectrometer, 15 minutes of the x axis represents 3600 pixels (1 pixel represents the ¼ seconds) and y axis represents 200 pixels. y axis represents the frequency.

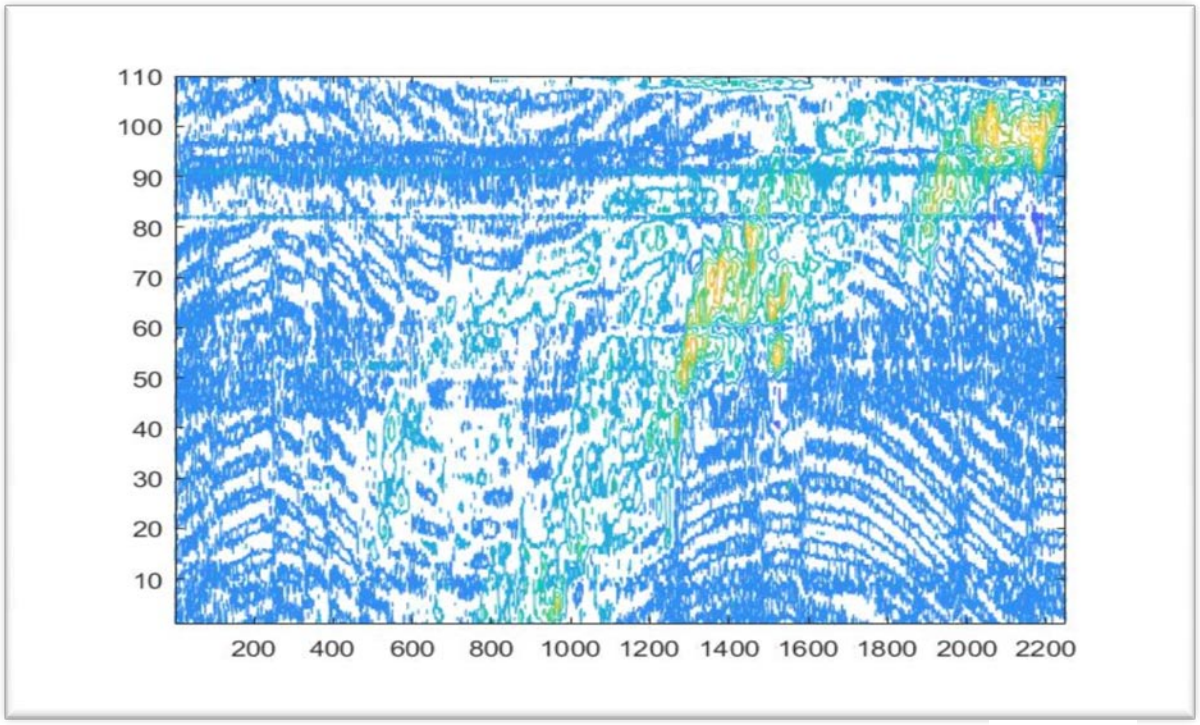

Figure 3.7: Contour plot of cropped flare

Then the cropped isolated flare was loaded to an array defined [C, I]. Here, C is maximum value of each column of the matrix and I is the frequency channel. Then the frequency channel vs time graph was plotted to identify the distribution of the frequencies with respect to the time as shown in the below Figure 3.8.

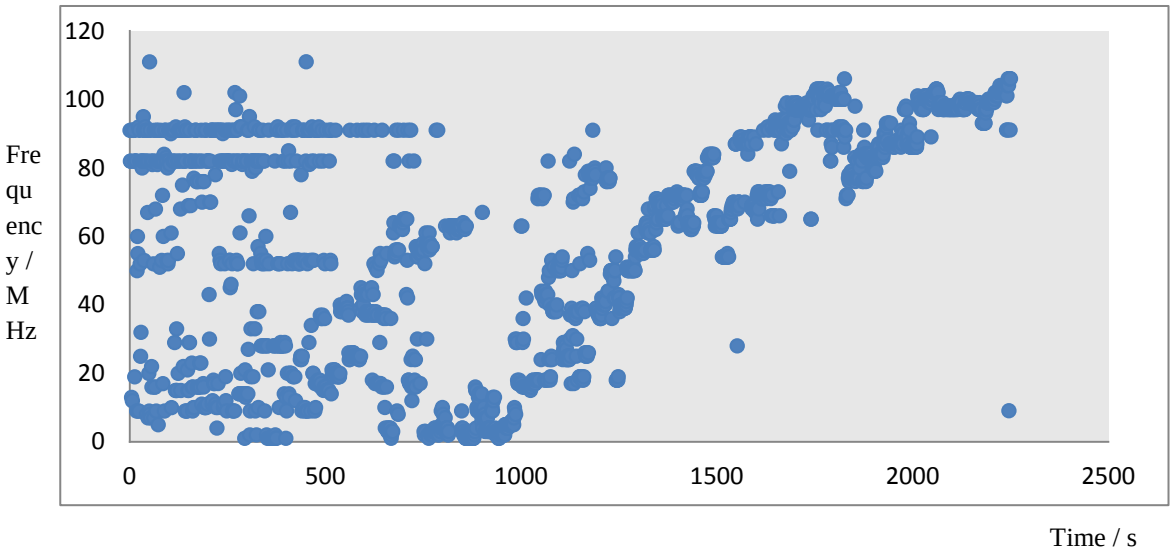

Figure 3.8: Frequency channel vs time graph with all points

There were many points which were not belong to the flare were recognized. Flare is spread in the time range of 700 to 2250 seconds. Therefore removed the points that were not belong to above time range. The final graph after removing the points was given in the figure 3.9.

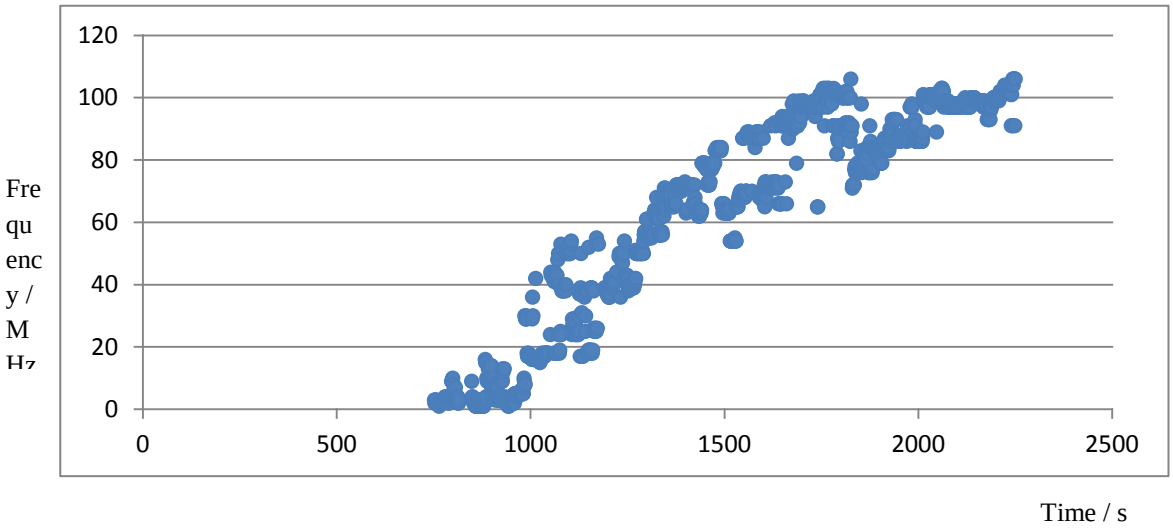

Figure 3.9: Frequency channel vs time graph with removed points

The values of the X axis and the Y axis of the image of solar radio burst lie between 1:3600 and 1:200 respectively as shown in Figure 3.6. After the image was cropped the value of the X axis was changed to 1:2250 and value of the y axis was changed to 85:195 as shown in Figure 3.7. So, the actual frequency values of the image were shifted to new values. Then it was transformed to actual values by using a code and frequency vs time graph was plotted as shown in figure 3.10.

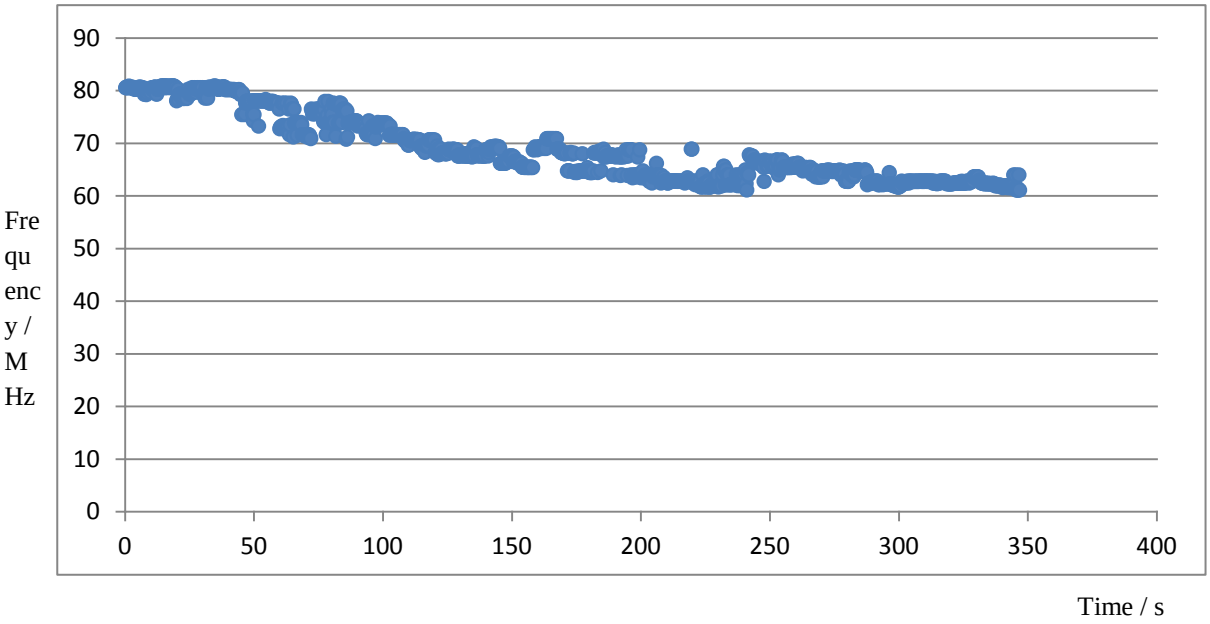

Figure 3.10: Frequency vs time graph after converted to actual frequency value

Generally, flare frequency is taken as the frequency of the starting point of the flare. For further calculations initial frequency was taken as the flare frequency (f value) and $\frac{df}{dt}$ was calculated for the initial point by using matlab software.

Finally, the values of f , $\frac{df}{dt}$, N and $\frac{dN}{dr}$ were substituted to the equation of shock speed that has been described in the Chapter 02. Different shock speeds were calculated for different distances, from the sun in the units of solar radius. The results for the uniform model are given in the Chapter 04.

3.2 Non-uniform electron density model

3.2.1 Analysis of electron density (N)

The values of C_1 , β and σ can be substituted to the equation 03 and can be rewritten as equation 06,

$$N(R, \beta) = N_Q(R) \{1+ 0.97\ e^{-[\frac{(x^2+(y-R)^2+z^2}{2\times(0.235)^2}]}\} \quad 3.1$$

To do the calculations for electron density of the non-uniform electron density model it is essential to find the point where the flare has started. This is needed because of the equation contains Cartesian coordinates with it. To find the point, an image with a whole solar disk needed to be taken. The image of the solar disc is in the 2D plane. Therefore it is necessary to convert the 3D equation (Equation 3.1) to 2D equation in-order to find the electron density. When 3D equation is converted to 2D, coordinates of the x and y axis remains and z axis becomes 0. The modified equation is given in equation 3.2.

$$N(R, \beta) = N_Q(R) \{1+ 0.97\ e^{-[\frac{(x^2+(y-R)^2}{2\times(0.235)^2}]}\} \quad 3.2$$

To calculate the electron density of the non-uniform electron density model, 2D image of a whole solar disc that corresponds to Figure 2.1, which has been captured by e-CALLISTO spectrometer on 2014/04/16, was taken. To identify the area where the flare has occurred, FITS files of series of images were taken to identify the exact image that shows the variation of the sun at the moment that the flare was occurred. Fits file which has been published by sdo.gsfc.nasa.gov website was used to take the 2D images of the sun. The FITS files were read using IRAF software and the images were obtained. When FITS file was read, it was shown by a matrix which consists of 1024×1024 pixels. Then the maximum intensity of the sequence of images at time from 19:48 to 20:12 were taken and noted as shown in the Table 3.1.

Table 3.1: Maximum intensity of the successive images for a given pixel coordinates

Time	Coordinates		Intensity Value
	X	Y	
19:48	138	369	594.44
19:50	138	369	537.75
19:52	138	369	414.75
19:54	138	369	386.44
19:56	439	449	6236.50
19:58	453	452	6297.62
20:00	454	452	10723.10
20:02	457	450	9166.25
20:04	458	450	10216.70
20:06	462	452	6549.75
20:08	455	448	7857.94
20:10	455	448	7134.62
20:12	455	448	4518.69

According to the data shown in the table 3.1 a graph was plotted with maximum intensity vs x coordinates. Accordingly plotted graph is given in the Figure 3.11.

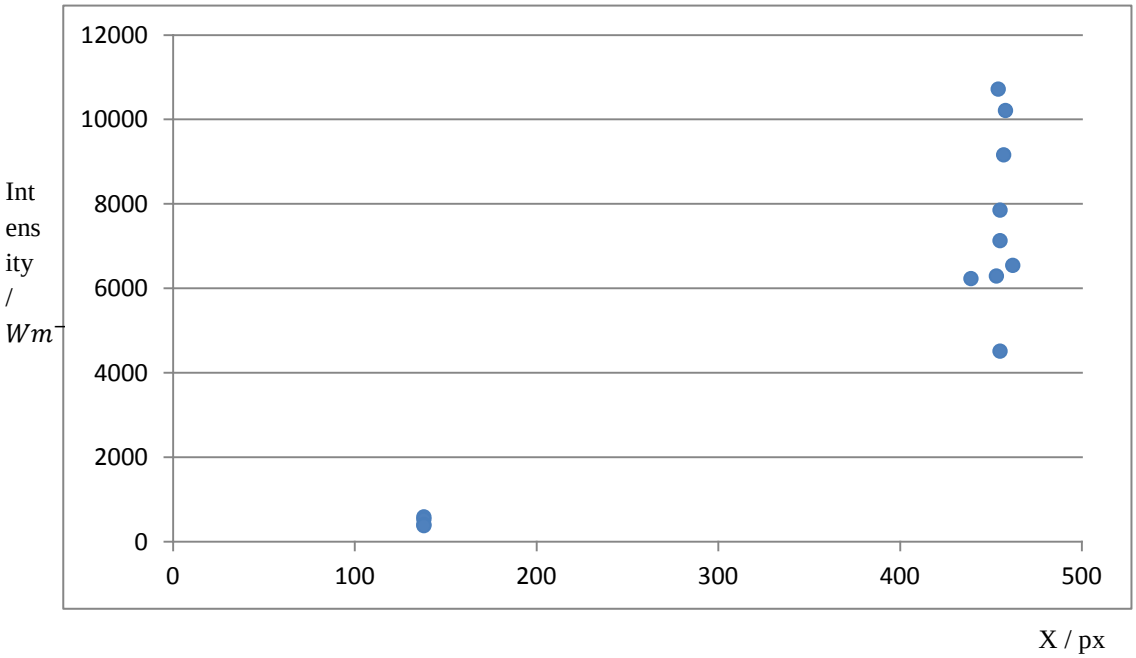

Figure 3.11: Maximum intensity vs x coordinate graph

In the above graph, point 454 of the x coordinate has the maximum intensity of 10723.1 and the coordinate of that point can be written as (454,452). Then by taking (454,452) as a reference point, further calculations done for different timeframes to confirm that the same point is the maximum. Accordingly calculated intensities are shown in the table 3.2.

Table 3.2: Intensities at the reference point (454,452)

X	Intensity Value
19:48	20
19:50	20.875
19:52	19.6875
19:54	23.375
19:56	105.5
19:58	5038.31
20:00	10723.1
20:02	4210.75
20:04	2478.19
20:06	1703.62
20:08	1652.69
20:10	1477
20:12	1203.81

Using the data shown in the above Table 3.2, graph (Figure 3.12) was plotted with the intensity vs time to identify the variation of the pixel values at reference point.

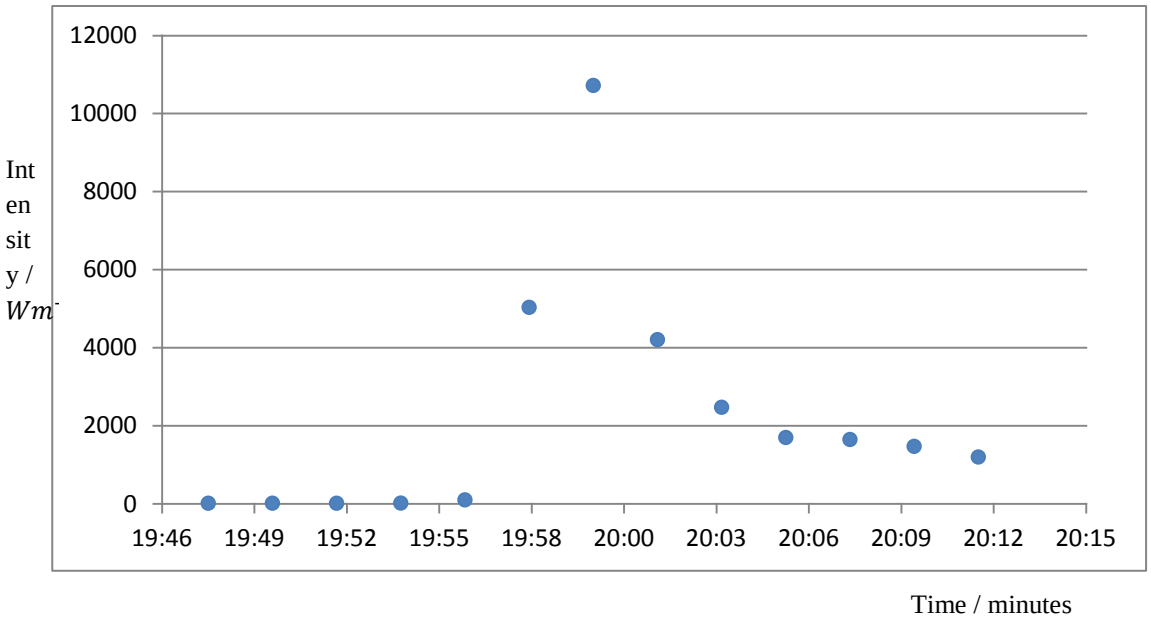

Figure 3.12: Intensity vs time graph

In the above graph the maximum intensity of 10723.1 is given at 20:00. To justify that the maximum intensity is given at 20:00, 5×5 error matrix for above all time frames were calculated as shown in below Figure 3.13. Sum of all values in the error matrix for each time frames were taken as the intensity and further calculations were done. Sum of intensities are shown below in Table 3.3.

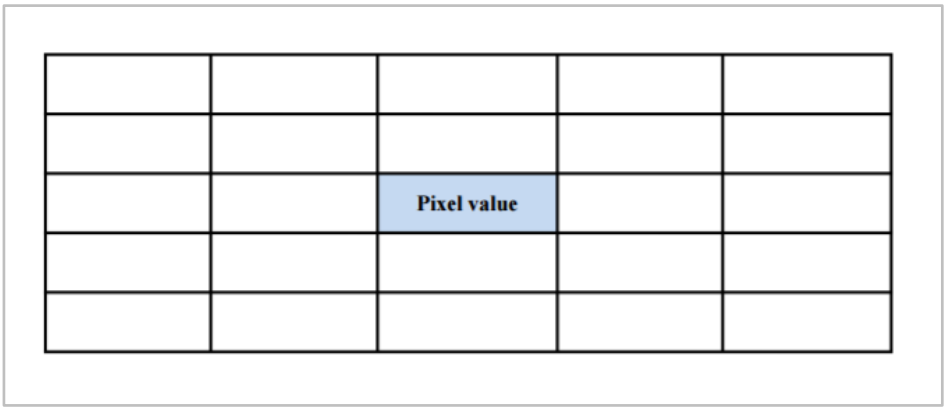

Figure 3.13: 5×5 error matrix

Table 3.3: Sum of intensities in the matrix

Time	Intensity Sum Value
19:48	587.5625
19:50	597.625
19:52	619.25
19:54	655.625
19:56	7142.378
19:58	58137.017
20:00	119537.712
20:02	92709.688
20:04	70314.255
20:06	52496.428
20:08	50536.52
20:10	45647.194
20:12	34831.002

Above data were used to plot a graph of sum of intensity vs time. The graph is shown in Figure 3.14.

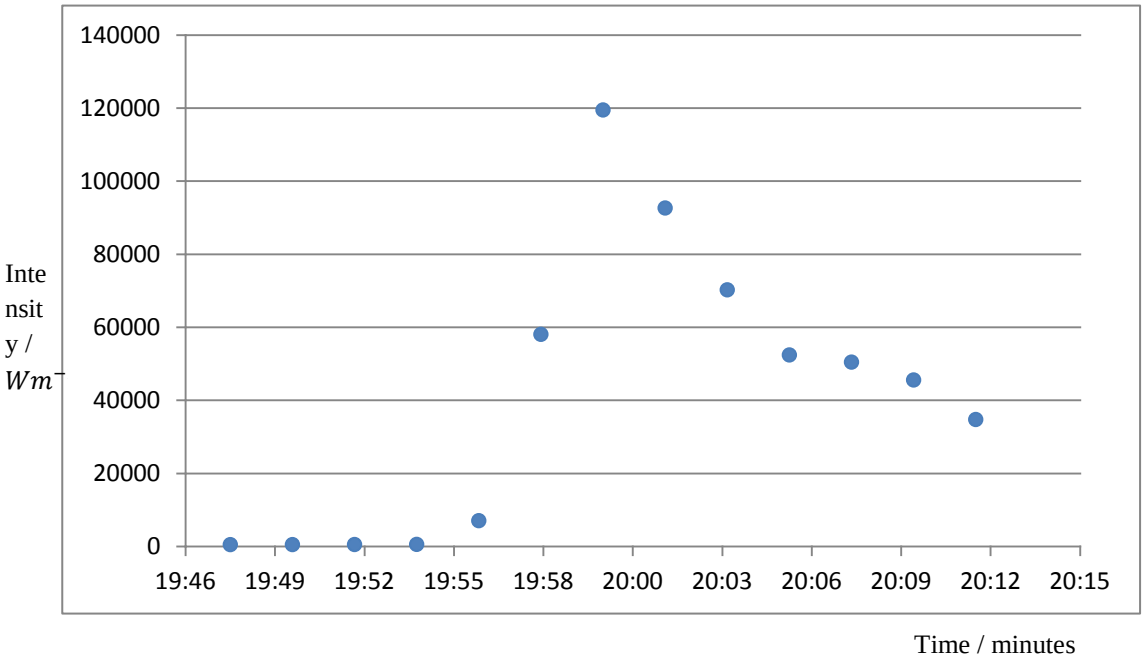

Figure 3.14: Sum of intensity vs time graph

The variation of intensity in the Figure 3.14 is similar to the variation in the Figure 3.12. Maximum value of the sum of intensity is 119537.712 and it is at 20:00. Image captured at 20:00 was taken as the exact image to calculate the coordinates because, when compared with the Figure 3.12 and 3.14 the same results were gained. The FITS file read by the IRAF software gives a gray colour image as shown in the Figure 3.15. The changed area of the sun is shown by the Figure 3.16.

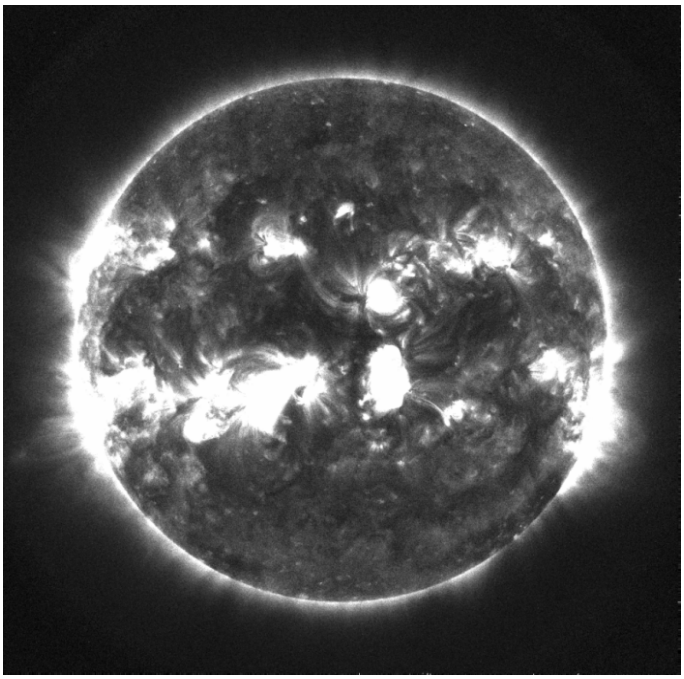

Figure 3.15: 2D image of sun

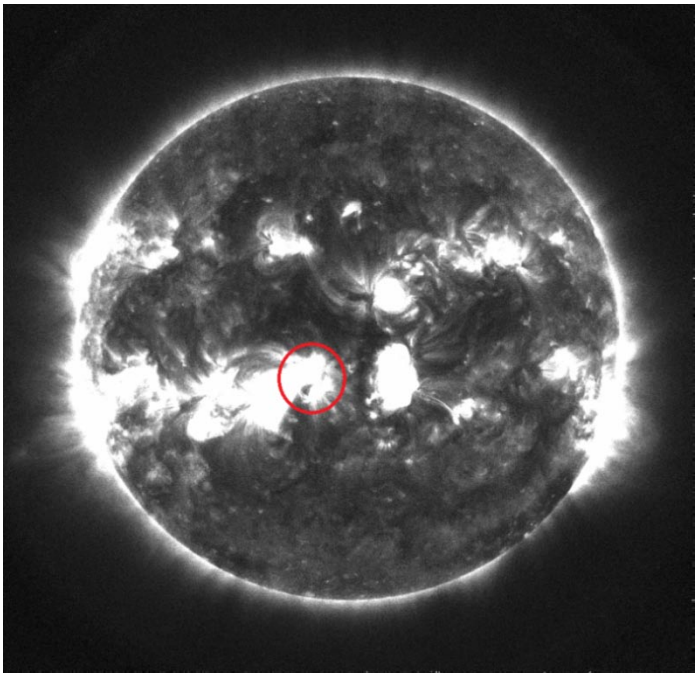

Figure 3.16: The area covered by red colour circle shows the changed area

The point that the flare has occurred is identified as (454,452) by considering the origin as a corner point of the image. Yet for the calculation, the origin should be shifted to the middle of the solar disc, since the modified electron density model has been introduced by considering the origin from the middle of the solar disc. Accordingly the previous origin is in the Figure 3.17 and the expected origin is shown in the Figure 3.18.

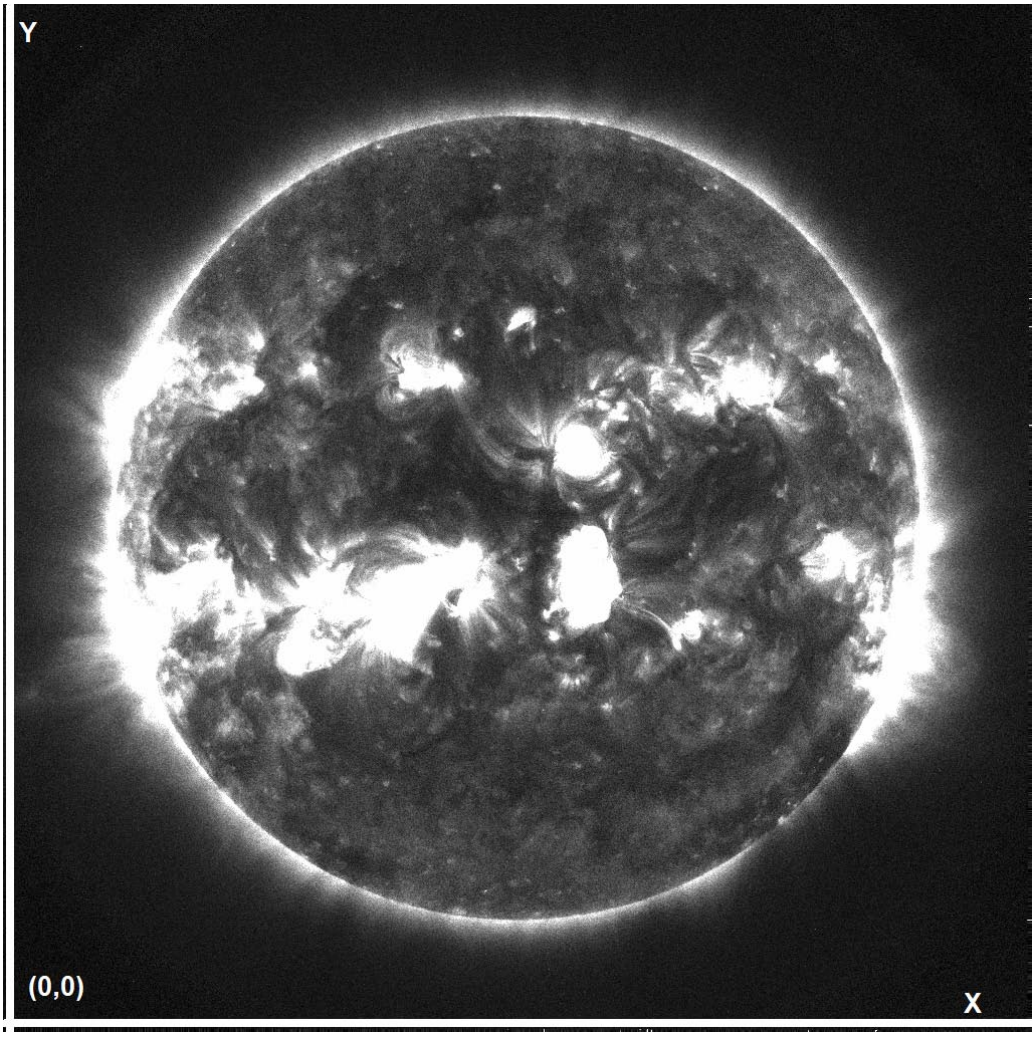

Figure 3.17: Previous origin by considering (0, 0) to be in the corner of the image

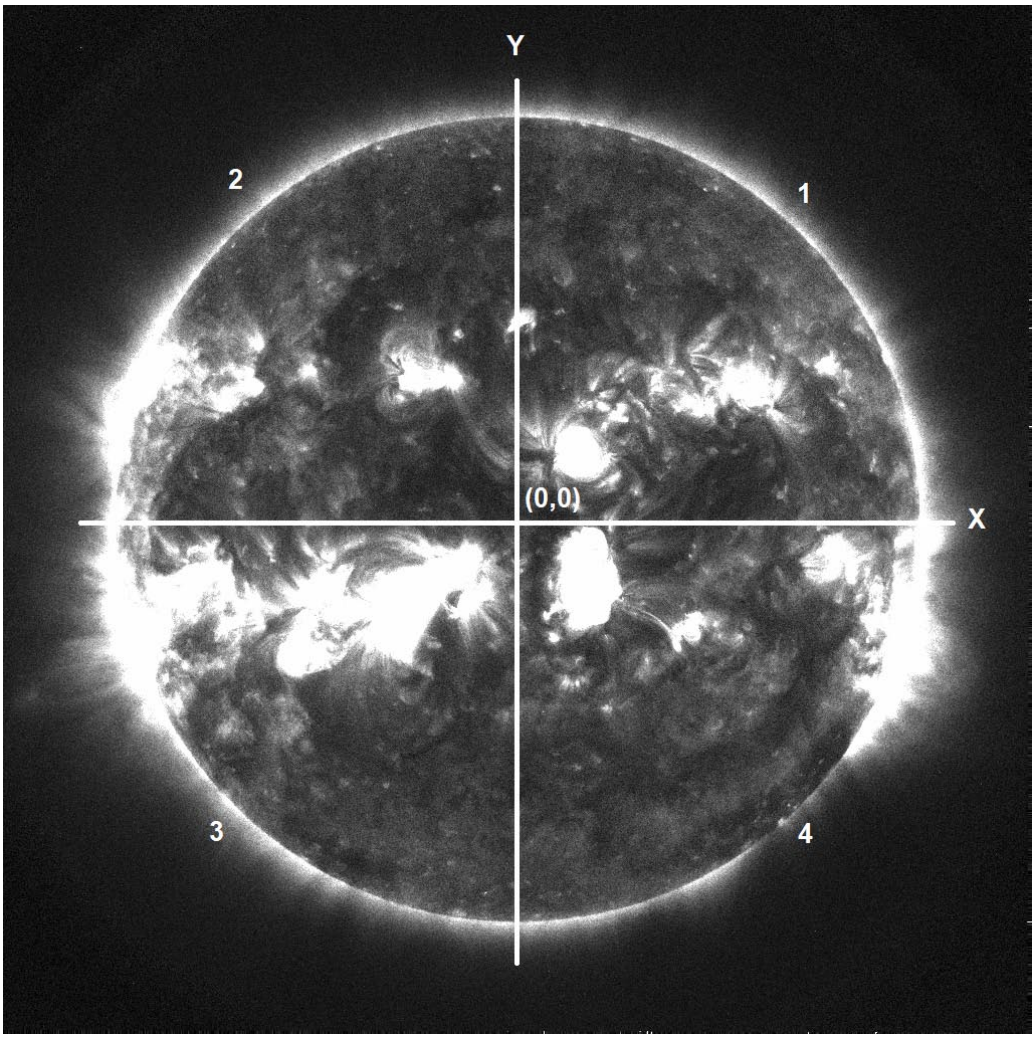

Figure 3.18: Expected origin considering (0,0) to be in the middle of the image

When consider the middle of the solar disc as the origin, the point that the flare occurred is available in the third quadrant of the Cartesian plane. Then, the values for both X coordinate and Y coordinate of that point become negative. If the image was loaded to the matlab software, the left side upper corner is normally taken as the origin as shown in Figure 3.19.

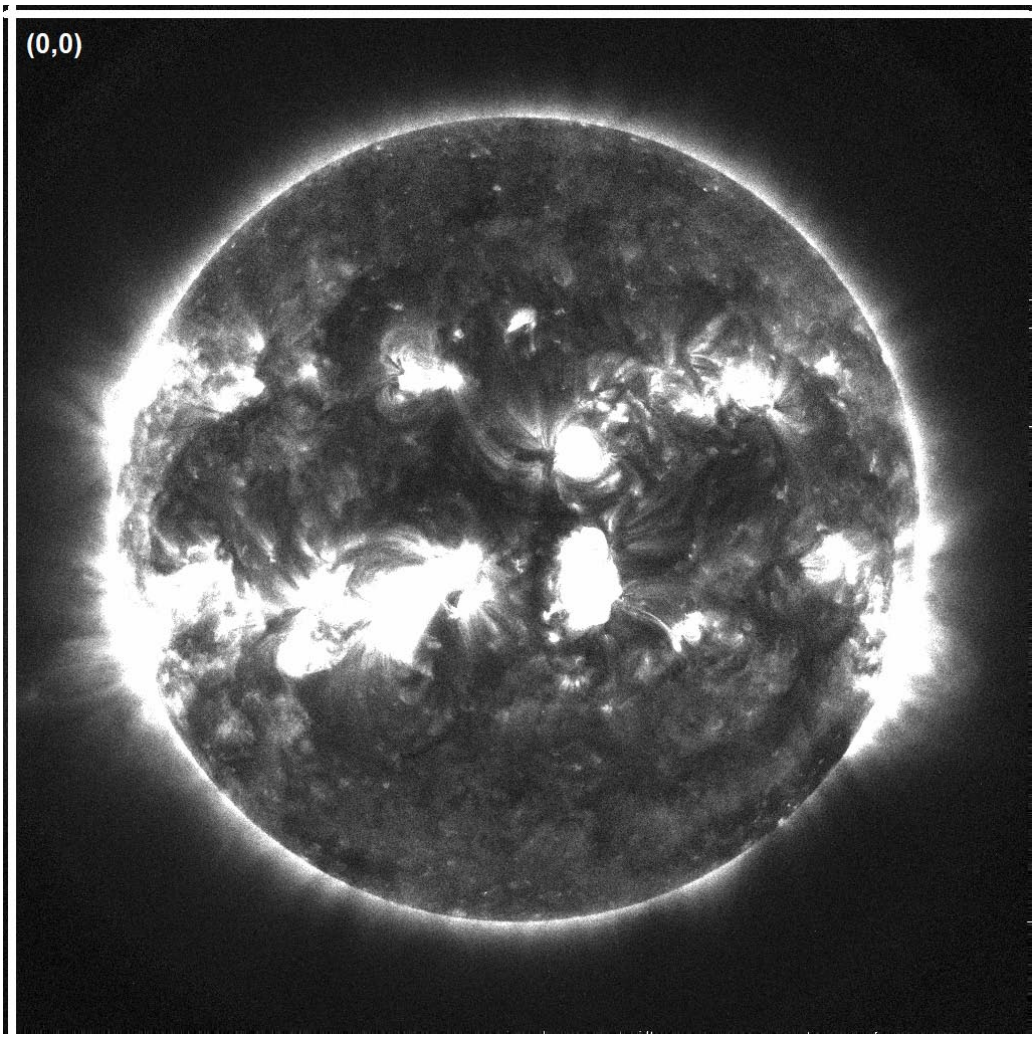

Figure 3.19: Origin of the image loaded to matlab software

When the origin was shifted to the center of the solar disc corresponding to the origin that was given by matlab software, the point that the solar flare occurred was shifted to the fourth quadrant of the Cartesian plane. The Figure 3.20 shows the variation. In order to clarify the error occurred by this change, the image was rotated in 270° degrees before the calculations were made. With the rotation, the point that the flare was occurred shifted back to the third quadrant. This is shown in the Figure 3.21.

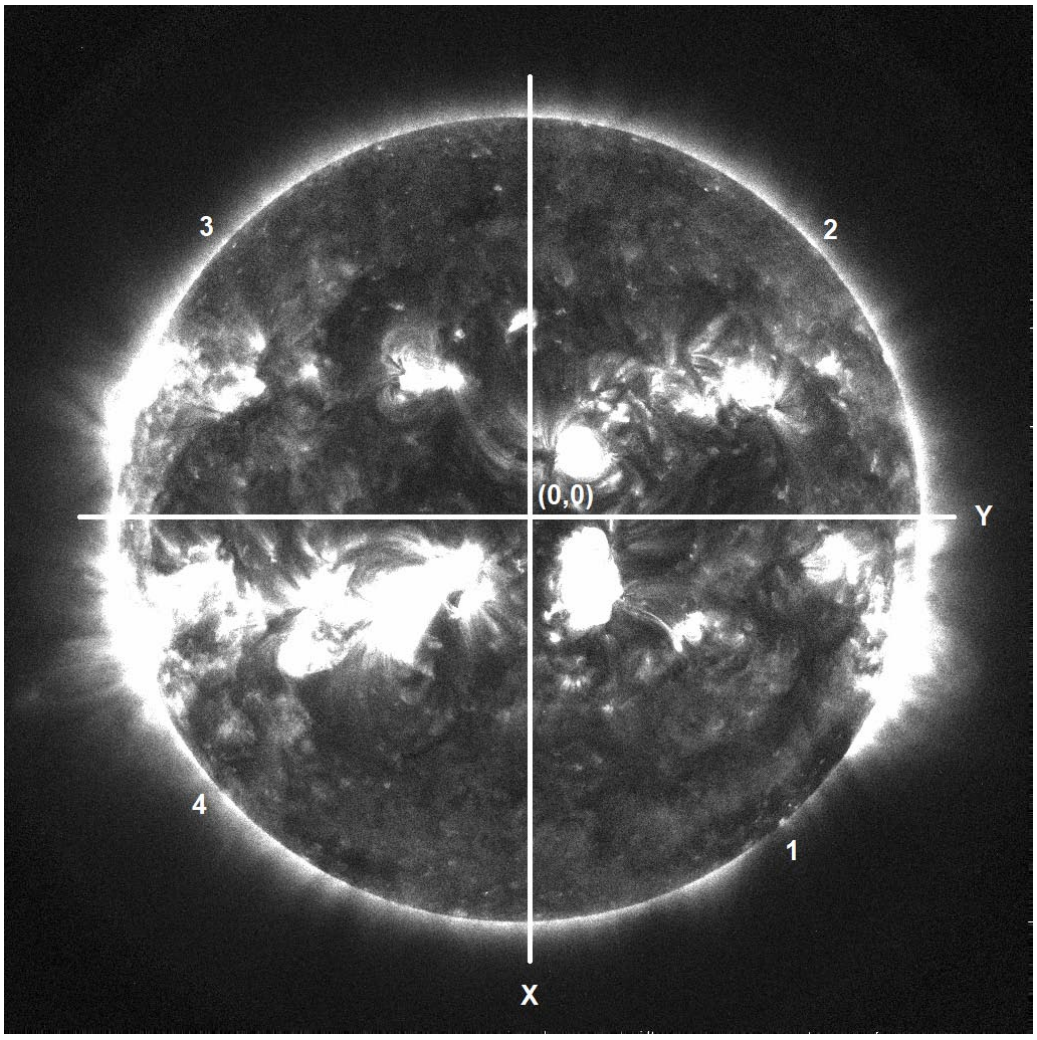

Figure 3.20: The point which the solar flare was occurred has been shifted to the fourth quadrant

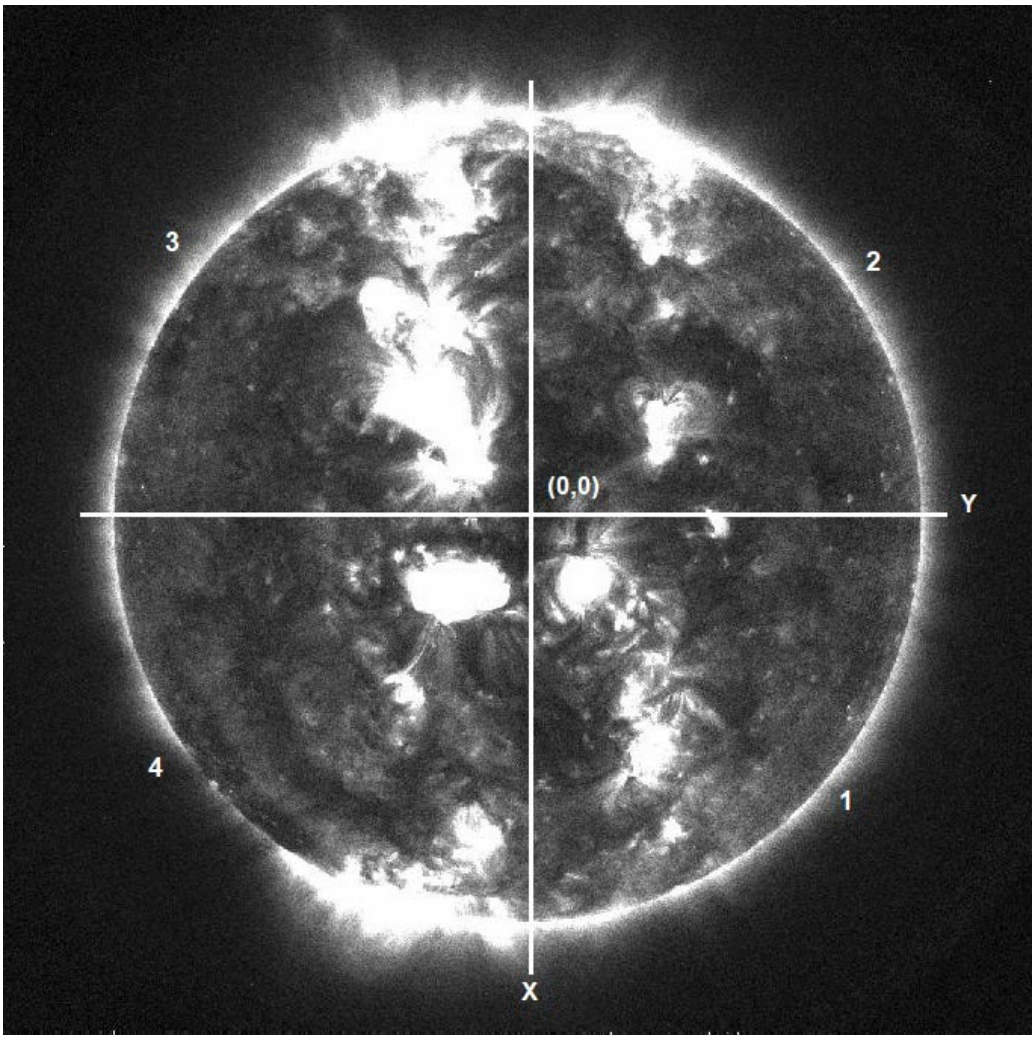

Figure 3.21: 270° degrees rotated image

The new pixel coordinates of the origin was tabulated by matlab and they are (523.307831102875, 500.564806364643). Hence the real coordinates of the point was calculated by subtracting the value (454,452) taken by IRAF software. Therefore the real coordinate of the point that the flare was occurred is given by (-69.3078311028750, -48.5648063646430). The minus sign is accounted for the fact that the flare has occurred in the third quadrant.

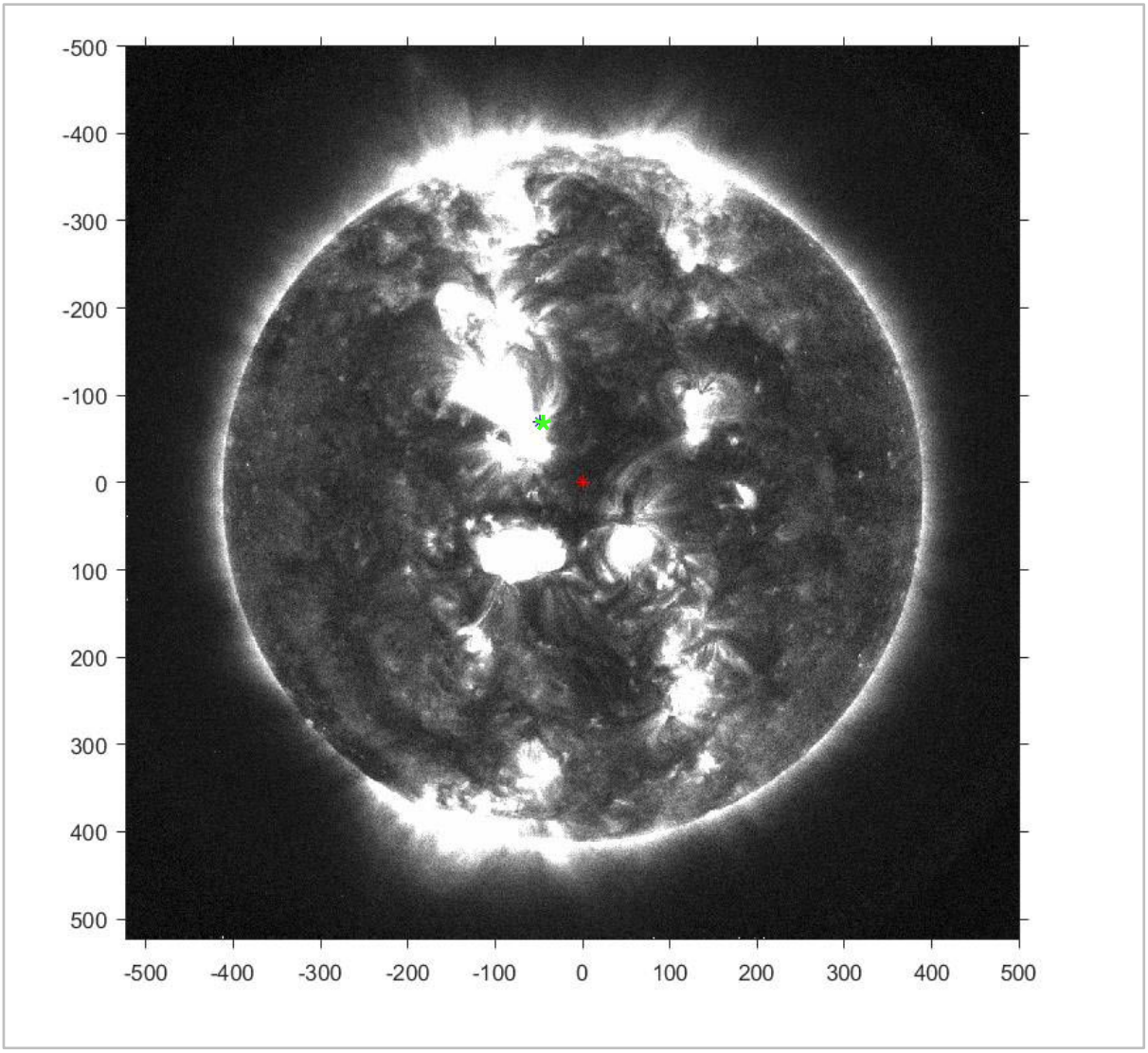

Figure 3.22: The point that is in red is where we have considered the origin and the point that is in green is the point that the flare has occurred

To find the β value, x and y coordinates should be transferred to the unit of solar radius. This was done by checking the ratio of the radius of the solar disc to the actual solar radius. After that by converting the amount of the solar radius denoted by 1 pixel value and multiplying that with the x and y values new coordinates were obtained in the unit of solar radius. Accordingly β value was calculated by using equation 2.5.

The β values were substituted in the equation 2.3 and electron density values for the different ‘ r ’ values were obtained. Then $\frac{dN}{dr}$ values were calculated considering the electron density as an exponential function because electron density of non-uniform electron density has been derived as an exponential function. Graphs of N vs r and $\frac{dN}{dr}$ vs r are shown below in the Figures 3.23 and 3.24.

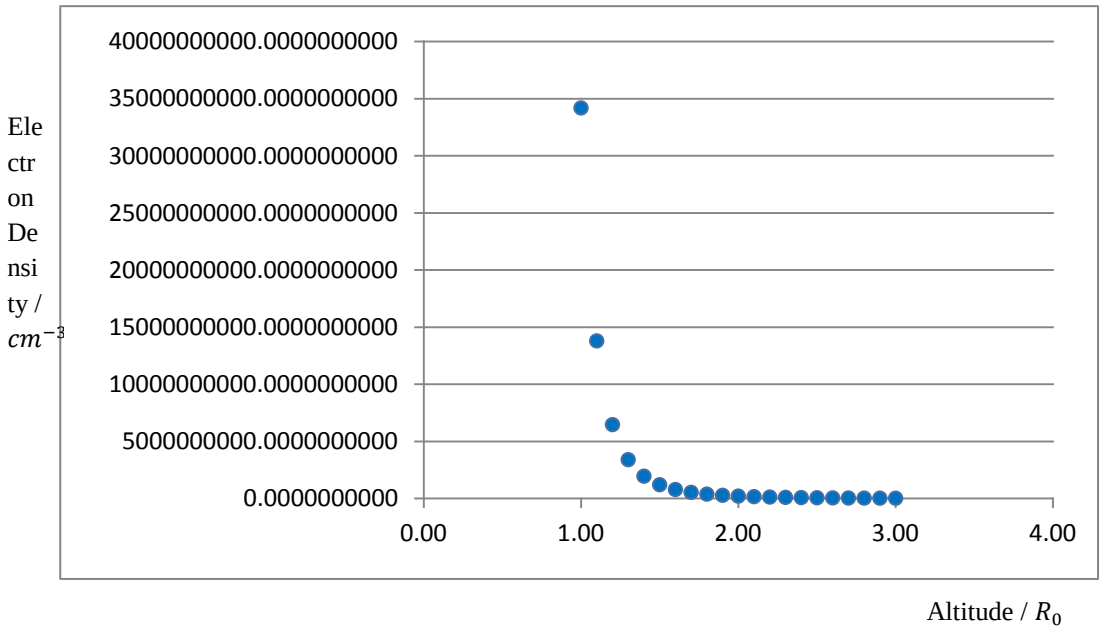

Figure 3.23: N vs r graph

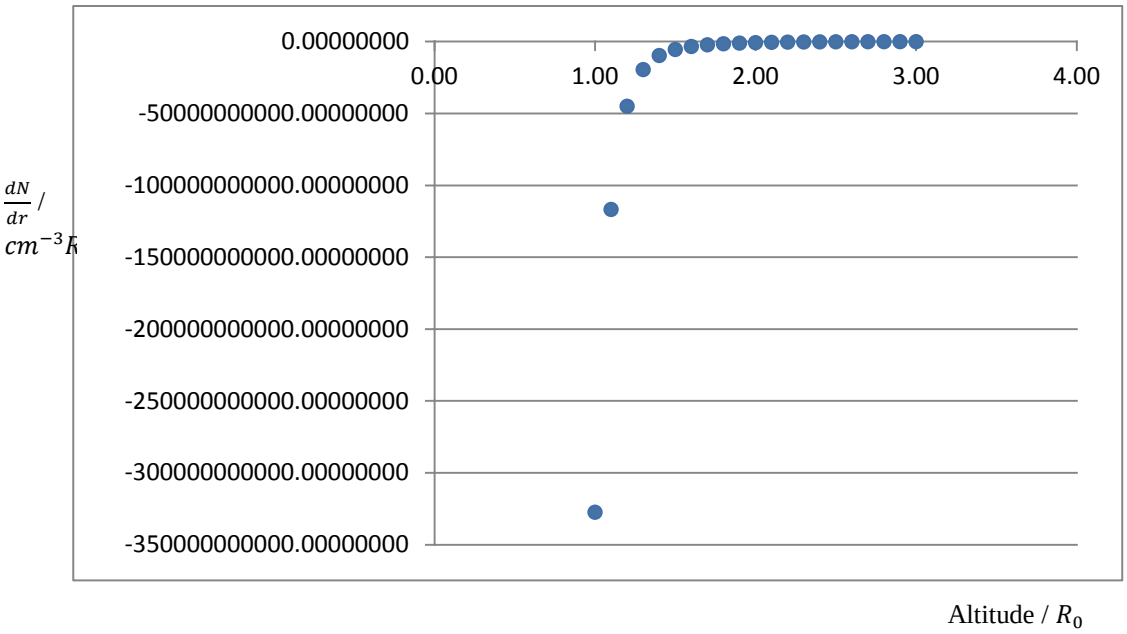

Figure 3.24: $\frac{dN}{dr}$ vs r graph

The values obtained for N and $\frac{dN}{dr}$ with the non-uniform density model were used in the calculation of shock speed given by the equation 2.1 and the results were given in the Chapter 04.

CHAPTER 04

RESULTS AND DISCUSSION

4.1 Shock speed for uniform density model

The graph of shock speed vs r tabulated from the results obtained for the shock speed of type II solar burst with the uniform density model as discussed in the Chapter 03 is given in the Figure 4.1. Figure 4.2 shows the same for the active sun as described by Newkirk.

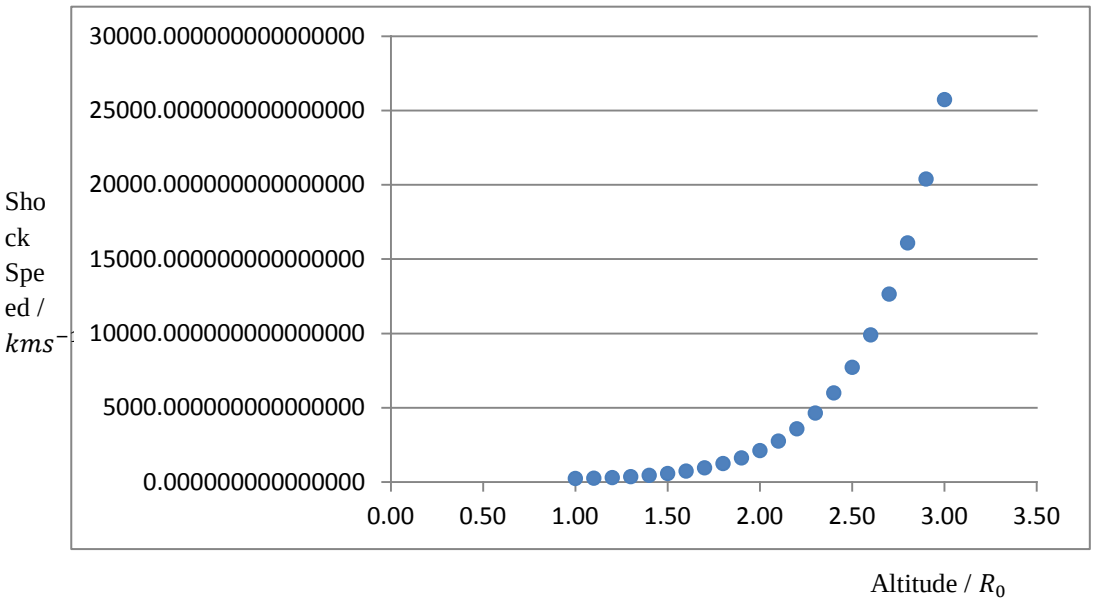

Figure 4.1: V vs r curve for uniform electron density model of quiet sun

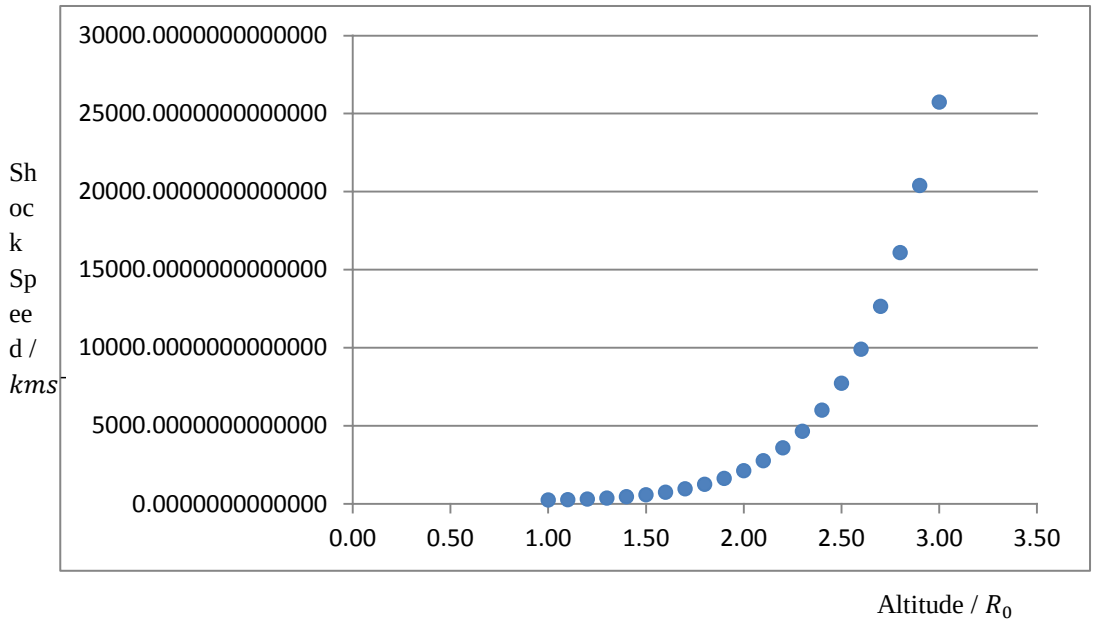

Figure 4.2: V vs r curve for uniform electron density model of active sun

According to the Figure 4.1 and 4.2, the behavior for the shock speed is similar for both active sun and the quite sun. Although the value of the electron density is 20 times higher in the active sun, the density variation $\frac{dN}{dr}$ (Figure 3.3) also higher in the active sun by giving the same value for the shock speeds for active and quite sun. This can be clearly seen with the equation 2.1.

4.2 Shock speed for non-uniform density model

The results obtained for the shock speed calculated from the non-uniform density model as described in the Chapter 03 and accordingly plotted graph of shock speed vs r is given in Figure 4.3.

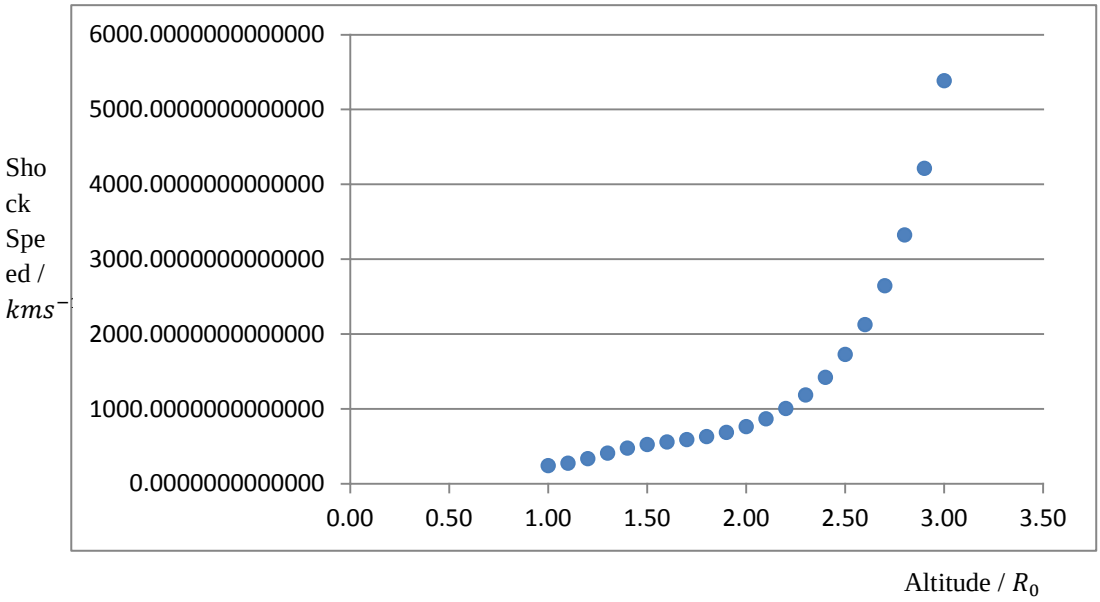

Figure 4.3: V vs r curve for non-uniform electron density model

In non-uniform electron density model, the increment for the speed is slow when compared with the uniform density model. Also, the velocity values for the non-uniform model are lower than that of the uniform model for the active sun. This is because the electron density values of the non-uniform model are higher than that of the active sun and the $\frac{dN}{dr}$ values also higher in the non-uniform model.

models

the density of the

4.4

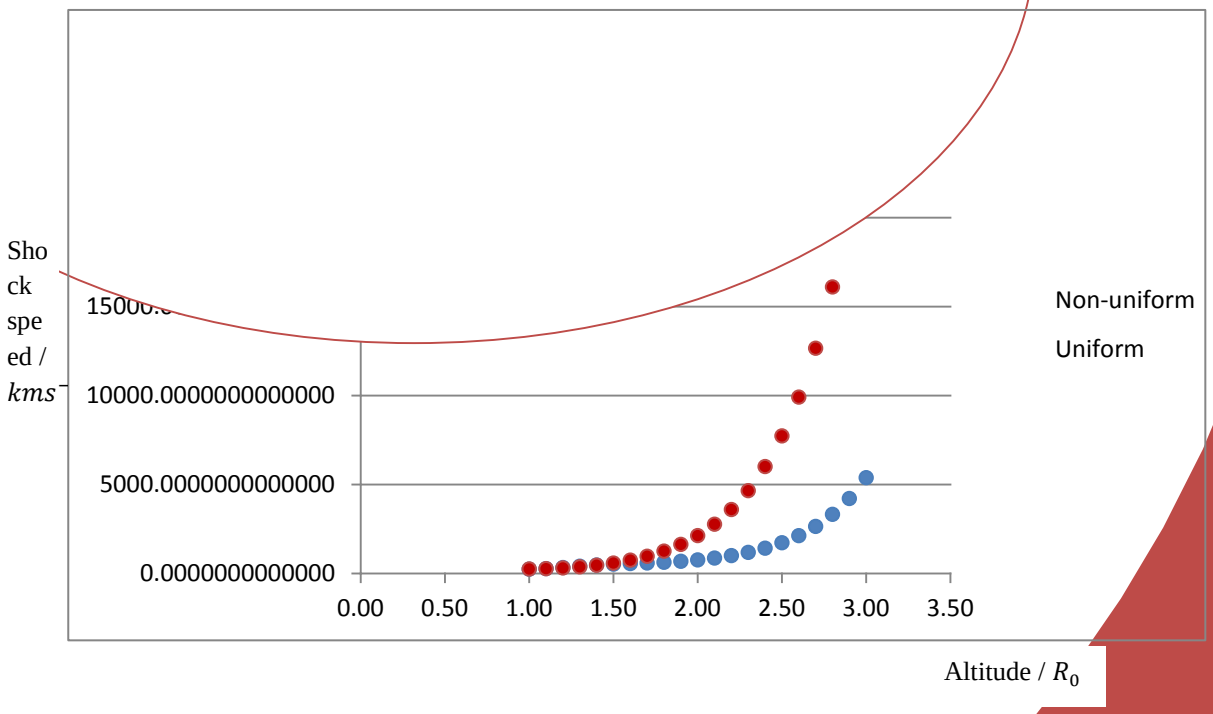

Figure 4.4: Velocity curves of uniform and non-uniform electron densit

The plot of velocities vs r tabulated from the uniform
odels shown in the Figure 4.4, demonstrate a sli
n 2.2 and 2.3 the electron densi

Therefore the shock speed for uniform electron density is quite higher than that of the non-uniform model. The change of the velocity starts from the 2.0 R_0 distance. In that point the shock speed of the uniform model is 2131 km/s and in non-uniform model it is 766 km/s. Although there are no clear evidences for the speed for the type II bursts using non-uniform density model, literature says that the typical shock speed is less than 1000 km/s in the above distance [10]. That is because the type II bursts are slow drift bursts. Therefore the value we obtained from the non-uniform electron density model is quite closer to the typical value. Hence we could conclude that the non-uniform density model is more appropriate for determining shock speed than the uniform electron density model. Nevertheless one need to clarify whether this is more appropriate with more sets of data obtained from e-CALLISTO global network. Therefore in future same type of calculations will be done for different sets of data in order to decide whether the study of shock speed of type II bursts can be done more accurately with the non-uniform electron density model by Newkirk.

REFERENCES

[1] J. V. Wijesekera, “Analysis of type II and type III solar radio bursts,” 2018.

[2] N. Zulaikha et al., “Implementation of Frequency Drift for Identification of Solar Radio Burst Type II,” vol. 6, no. 5, pp. 775–780, 2016.

[3] L. Sui, “Modeling Solar Flare Hard X-ray Images and Spectra Observed with RHESSI,” no. January, 2005.

[4] G. D. Holman et al., “Implications of X-ray Observations for Electron Acceleration and Propagation in Solar Flares,” Space Sci. Rev., vol. 159, no. 1–4, pp. 107–166, 2011.

[5] N. H. Zainol, Z. S. Hamidi, N. N. M. Shariff, S. Arifin, and C. Monstein, “Investigation of Drift Rate of Solar Radio Burst Type II Due To Coronal Mass Ejections Phenomenon,” Int. Lett. Chem. Phys. Astron., vol. 48, no. i, pp. 146–154, 2015.

[6] R. Beck, "SOLAR ASTRONOMY HANDBOOK", 1995.

[7] M. Zeilik and J. Gaustad, Astronomy, the cosmic perspective, 2nd ed. New York: Wiley, 1990.

[8] A. O. Benz et al., “A World-Wide Net of Solar Radio Spectrometers: e-CALLISTO,” Earth, Moon Planets, vol. 104, no. 1–4, pp. 277–285, 2009.

[9] S. White, “Solar Radio Bursts and Space Weather,” Asian J. Phys, vol. 16, pp. 189–207, 2007.

[10] C. Monstein, “Catalog of dynamic electromagnetic spectra observed with Callisto , Phoenix-3 and ARGOS,” pp. 1–16, 2013.

[11] A. Krüger, Introduction to solar radio astronomy and radio physics. Dordrecht: D. Reidel, 1979.

[12] C. Monstein, "e-Callisto solar spectrometer", E-callisto.org, 2018. [Online]. Available: http://e-callisto.org/. [Accessed: 16- Dec- 2018].

[13] M. Hanslmeier, A., & Messerotti, MOTIONS IN THE SOLAR ATMOSPHERE, vol. 239, no. 9. 1999.

[14] G. Newkirk, “THE SOLAR CORONA IN ACTIVE REGIONS AND THE THERMAL ORIGIN OF THE SLOWLY VARYING COMPONENT OF SOLAR RADIO RADIATION.”